Dissertation

Maximum Power Point Tracking of a DFIG Wind Turbine System

Graduate School of
Natural Science & Technology
Kanazawa University

Division of
Electrical and Computer Engineering

Student ID No.: **1424042007**

Name: **Phan Dinh Chung**

Chief advisor: *Prof.* **Shigeru YAMAMOTO**

Date of Submission: January 6, 2017

Abstract

Doubly-fed induction generator (DFIG) has been used popularly in variable speed wind turbines because the DFIG wind turbine uses a small back-to-back converter to interface to the connected grid, about 30% comparing to the wind turbine's capacity, and provides a control ability as good as a variable speed wind turbine using a generator with a full converter. The most important purpose of a variable speed wind turbine or a DFIG wind turbine, in general, is to utilize fully the kinetic energy of wind for electric generation. To meet this objective, several publications provided different methods. Generally, the previously proposed schemes can be listed into two groups including wind speed-based method and wind speed sensorless one. With the first group, the wind turbine can give a good performance in tracking maximum power point but it requires a precise and instantaneous wind speed measurement; this requirement hardly achieve in practice. With methods in the second group, an anemometer does not require but the wind turbine using these methods cannot track maximum power point efficiently under varying wind conditions.

In this dissertation, I proposed two methods and control laws for obtaining maximum energy output of a doubly-fed induction generator wind turbine. The first method aims to improve the conventional MPPT curve method while the second one is based on an adaptive MPPT method. Both methods do not require any information of wind data or wind sensor. Comparing to the first scheme, the second method does not require the precise parameters of the wind turbine. The maximum power point tracking (MPPT) ability of these proposed methods are theoretically proven under some certain assumptions. In particular, DFIG state-space models are derived and control techniques based on the Lyapunov function are adopted to

derive the control methods corresponding to the proposed maximum power point tracking schemes. The quality of the proposed methods is verified by the numerical simulation of a 1.5-MW DFIG wind turbine with the different scenario of wind velocity. The simulation results show that the wind turbine implemented with the proposed maximum power point tracking methods and control laws can track the optimal operation point more properly comparing to the wind turbine using the conventional MPPT-curve method. The power coefficient of the wind turbine using the proposed methods can retain its maximum value promptly under a drammactical change in wind velocity while this cannot achieve in the wind turbine using the conventional MPPT-curve. Furthermore, the energy output of the DFIG wind turbine using the proposed methods is higher compared to the conventional MPPT-curve method under the same conditions.

Contents

List of Figures

List of Tables

Acknowledgement

Firstly, I would like to express my thanks to Prof. Shigeru YAMAMOTO who has opened a chance for me to pursue this doctoral course and helped me to effectuate this research. I got a variety of new knowledge and experience from Prof and his lab. I also want to thank Prof. Osamu KANEKO who supported me many things in research.

Secondly, I want to say thank you for Vietnam International Education Development - Ministry of Education and Training who support financially for me to pursue this research. I also want to say thank you to Dr. Tran Vinh Tinh and Associate Prof. Dinh Thanh Viet, leaders of Electrical engineering Department-Danang University of Science and Technology, who gave me time for this PhD course.

Next, I would like to say thank you to all members of my family, parents and siblings, who always encourage me to study. In particular, thanks for the help of my brothers and sisters in taking care my parents, I can be assured to concentrate on studying.

Last but not least, I want to thank you for sharing knowledge from all members of MoCCoS laboratory, Mr. Mohd Syakirin, Mrs. Dessy Novita, and Mr.Herlambang Saputra. I want to thank Mr. Kyohei Asai, my tutor, who help me to get on well in daily life in Kanazawa. By the way, I also thank all friends who shared everything in daily life.

Phan Dinh Chung

Kanazawa, January 2017

Chapter 1

Introduction

The fossil-fuel exhaustion and environment pollution concerns have urged researchers to utilize renewable energy resources such as the wind, solar, and wave energy for generating electricity. Until now, the use of wind energy for electric generation has been developing in many countries; many large-scale wind farms, both offshore and onshore, have been built and exploited. According to Global Wind Energy Council (GWEC) [1], over 80 countries in the world have been utilizing wind energy for electricity generation with installed wind capacity in total up to 433GW at the end of 2015 and 14 of these countries, installed capacity in total is over 5000MW. Referring to the prediction of GWEC, the total wind capacity data will increase to 792GW at the end 2020. We always expect that electric energy withdrawing from a wind turbine system should be as high as possible. In other words, we should utilize fully wind energy for electric generation from a wind turbine.

To optimally utilize wind energy, the energy conversion efficiency of wind turbines must reach the utmost limit. Therefore, maximum power point tracking (MPPT) is an essential target in wind turbine control. To track the maximum power point, the rotor speed of the wind turbine/generator should be adjustable. Hence, the concept of a variable-speed wind turbine (VSWT) was proposed. According to [2, 3, 4, 5], when the generator in a VSWT operates at variable speeds, its output is often synchronized with the grid via a converter system. Depending on the type of generator used in the VSWT, the converter's size will vary as shown in Fig.1.1. With VSWT based on synchronous generator (SG), permanent magnetic

synchronous generator (PMSG), or squirrel-cage induction generator (SCIG), the generator is interfaced to grid through a converter as Fig.1.1a; during operation, all active power generated by the generator is transfered to the connected grid and hence, a full converter whose capacity should not be smaller than the generator-wind turbine's capacity is used [3, 4, 5]. However, for VSWT that use a doubly fed induction generator (DFIG) in Fig.1.1b, a partial converter is required on the rotor side [2] because the power generated/absorbed on the rotor side is around 30% of the DFIG-wind turbine capacity. In other words, compared to a full converter-based VSWT, the use of a DFIG wind turbine is more economical; in fact, DFIG wind turbines are more frequently used in large wind farms. Therefore, control for a MPPT target in DFIG-based wind turbines has become an interesting topic.

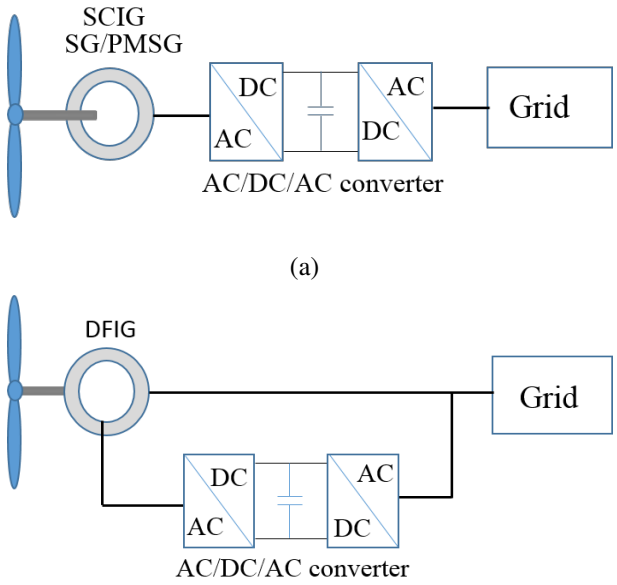

Fig. 1.1: Variable speed wind turbine based on: (a) full power converter and (b) partial power converter.

To track the maximum power point during operation, a wind turbine must be generally equipped with a good controller integrated with a comprehensive MPPT algorithm. Many MPPT methods have been proposed [5, 6, 7, 8, 9, 10, 11, 12, 13]. Original methods are based on the characteristic curve. They use the curve of the optimal power versus wind speed, for example, or the optimal tip-speed ratio of a

wind turbine and wind data to determine the reference signal for the controller [8, 6]. These methods are called wind-data-based methods. Generally, with wind-data-based methods, the MPPT ability of a wind turbine is appreciably high if accurate wind data is available. However, because of the rapid natural fluctuation of wind, wind speed measurement is hardly reliable [14]. To overcome this drawback, other methods such as the MPPT-curve method [11, 12, 10, 13] and perturbation and observation (P&O) method [7] were suggested. They operate basically on the output of the generator; hence, they are called wind speed-sensorless methods. Compared to the wind-data-based methods, the wind speed-sensorless methods cannot track the optimum point as efficiently as [15]. However, this method is often implemented in wind turbines because there is no requirement for an anemometer. The P&O method is originally applied for extremum seeking in small inertia systems such as photovoltaic power systems or small-size PMSG wind turbines with a DC/DC converter [5, 7]. Unlike the P&O method, the MPPT-curve method, which indexes the current power output (or rotor speed) as well as the wind turbine's MPPT curve to determine the reference rotor speed (or power output) [11, 12, 13], can apply to both large- and-small scale wind turbines; it is more efficient and does not require any perturbation signal [8]. However, for the high inertia of a generator wind turbine system, a wind turbine using the MPPT-curve method cannot track the maximum point as rapidly as a wind turbine using the wind-data-based method [15].

In terms of designing the controller for a wind turbine, traditional proportional-integral (PI) control is used for many purposes, including rotor-speed, current, and power control [11, 12]. A drawback of PI control is that stability is not theoretically guaranteed [16, 17]. Thus, sliding-mode control has been recently developed [18, 19, 20, 21, 22]. In fact, sliding-mode control has been applied to the rotor speed [20, 21, 22]. However, wind speed measurement is prerequisite for sliding mode control.

This research suggests two new schemes to maximize the energy output of a DFIG wind turbine without any information about the wind data or an available anemometer. These proposed schemes are based on the improvement of the wind turbine's MPPT curve and the adaptation of MPPT curve; their names are improved

MPPT-curve method and adaptive MPPT method. Certainly, the improved MPPT-curve method is completely independent to the adaptive MPPT method. In addition to the proposed MPPT methods, in this research, two new controllers based on Lyapunov control theory will be designed for power and rotor speed adjustment purposes, corresponding to the improved and adaptive MPPT method. The efficiency of the proposed schemes will be verified, analyzed, and compared with the conventional MPPT curve method with PI controllers by the simulation of a 1.5-MW DFIG wind turbine in a MATLAB/Simulink environment.

1.1 Outline of The Dissertation

This dissertation is organized as follows.

In Chapter 2: DFIG-wind turbine

In Chapter 3: Controller design and proposed MPPT schemes

In Chapter 4: Simulation results and discussion

In Chapter 5: Conclusion

Appendix A

Appendix B

Chapter 2

DFIG-Wind Turbine

As we mentioned in Chapter 1, DFIG-wind turbines are produced popularly in middle and large capacity scale, from several hundred kilowatts to several megawatts. A DFIG wind turbine consists of two main components including a wind turbine and doubly fed induction generator (DFIG) [23]. The wind turbine aims to absorb kinetic energy from wind and produces mechanical torque to rotate its shaft. In normal operation, the wind turbine's velocity range is several rpm [24] while the DFIG's rotational speed varies from several hundred to thousand rpm depending on the number of pole pairs. Hence, the wind turbine is linked to the DFIG through a shaft system including a turbine shaft, generator shaft, and gearbox (GB), as shown in Fig.2.1. Through this shaft system, the mechanical energy on the turbine shaft is transferred to the generator in order to convert to electrical energy. In this research, this shaft system is a union mass. It means there is not energy losses on the shaft system. Generally, the dynamic equation for a generator-wind turbine system [18] is used to described

$$J\frac{d}{dt}\omega_r(t) = T_m(t) - T_e(t), \tag{2.1}$$

where, J is the inertia of the generator-wind turbine system; ω_r is the rotor speed of the wind turbine; T_m and T_e respectively stand for the mechanical torque of the wind turbine and the electrical torque of the generator referring to the turbine speed.

Moreover, to use the mechanical and electrical power P_m and P_e, respectively,

we can rewrite (2.1) as

$$J\omega_r(t)\frac{d}{dt}\omega_r(t) = P_m(t) - P_e(t). \tag{2.2}$$

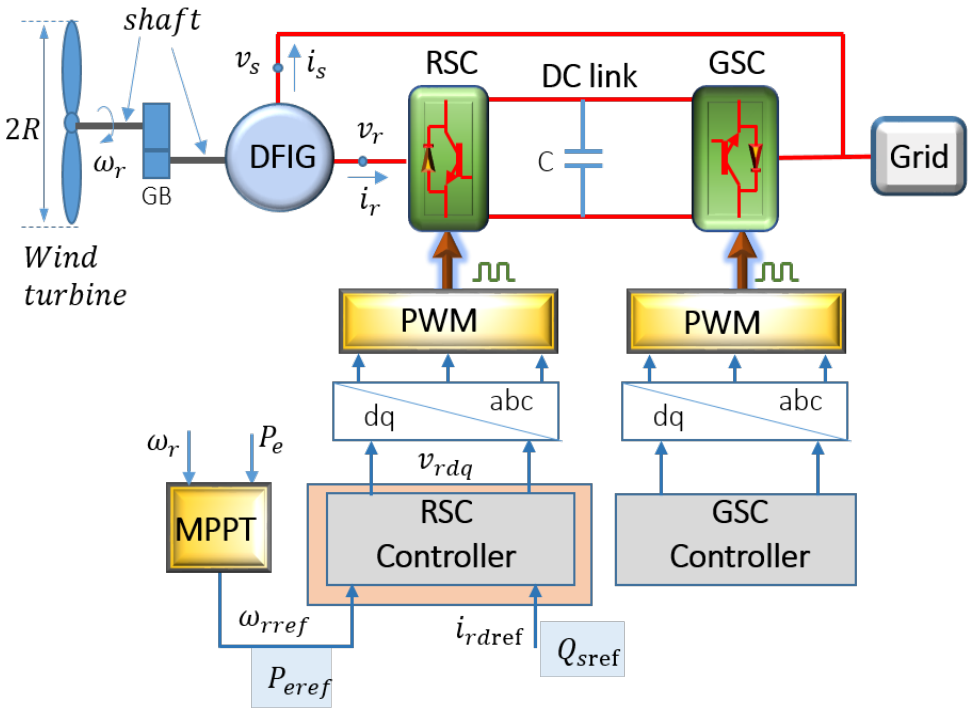

Fig. 2.1: Overall system of the doubly-fed induction generator (DFIG) wind turbine.

The purpose of the DFIG is to convert the mechanical energy on its shaft to electric energy on both stator and rotor winding. Generally, DFIG is an induction generator like a SCIG but its rotor winding is not shorted-circuit and is connected to an external grid. During operation, the DFIG must receive reactive power from external grid through the stator or rotor winding to produce flux in the DFIG; the electric frequency on the stator winding depends on the frequency of the external grid while the electric frequency on the rotor side depends on the generator's rotational speed. Hence, when the DFIG-wind turbine operates in variable speed, the frequency on the rotor side varies among wind speed; to interface to a connected grid, the stator side of the DFIG is often connected directly to the grid whereas the rotor side is connected through a back-to-back converter. The main objective of the back-to-back converter is to synchronize between the rotor winding and the

connected grid. General speaking, the back-to-back converter includes a rotor-side converter (RSC), grid-side converter (GSC), and DC link. In the DFIG-wind turbine, since the rotor side can supply/absorb active power to/from the connected grid, the RSC (GSC) can work as either a rectifier (inverter) or an inverter (rectifier). This is reason why a bidirectional or back-to-back converter using IGBT-valves must be installed on the rotor side. Furthermore, the slip speed of the DFIG is only from -30% to 30% so the maximum power flowing through the back-to-back converter is around 30% of DFIG capacity. Therefore, the converter capacity is around 30% of DFIG capacity and this is a good point of DFIG-wind turbine.

For the DFIG wind turbine, thanks to the back-to-back converter, the DFIG-wind turbine gives a qualified control ability. Through the RSC, we can adjust the turbine speed to achieve a desired power and adjust both reactive power quantity and direction on the stator side. The GSC is often controlled to remain a constant DC voltage on the DC link and to support reactive power to the connected grid. To be more convenient in designing controllers, a dq frame is often used and all three phase signals such as current and voltage are converted from an abc frame to the dq frame. Hence, the output of the controllers must be converted from the dq frame to the abc frame, in Fig.2.1, and then pulse-wide-modulations (PWMs) generate pulses to switch on/off IGBT-valves in RSC and GSC.

In this research, we only focus on designing the RSC controller and proposing MPPT method. Therefore, in this chaper, we only describe the mathematical modeling of the wind turbine and the DFIG.

2.1 Wind turbine

As we know, the wind turbine is to absorb kinetic from wind through its blade system and convert it to mechanical energy on its shaft. When the turbine rotates at ω_r and wind speed is V_w, the tip speed ratio is defined by

$$\lambda(\omega_r, V_w) \triangleq \frac{R\omega_r}{V_w}, \tag{2.3}$$

where R is the length of its blade. Mechanical power on its shaft P_m is written as

$$P_m(\lambda, V_w) \triangleq \frac{1}{2}\rho\pi R^2 C_p(\lambda,\beta)V_w^3, \tag{2.4}$$

where ρ, and $C_p(\lambda,\beta)$ are the air density, and power coefficient, respectively. The power coefficient C_p represents the energy conversion efficiency of the wind turbine and generally depends on both the tip speed ratio λ and the pitch angle β. Normally, the $C_p(\lambda,\beta)$ depends on the manufacture of the wind turbine and it has a maximum point respecting to λ at a constant β.

By using (2.3), (2.4) becomes

$$P_m(\omega_r, V_w) = \frac{1}{2}\rho\pi R^5 \frac{C_p(\lambda,\beta)}{\lambda^3}\omega_r^3. \tag{2.5}$$

For example, a 1.5MW wind turbine with

$$C_p(\lambda,\beta) = (\frac{79.254}{\lambda_i} - 1.5\beta - 5.315)e^{-21/\lambda_i} + 0.009\lambda, \tag{2.6}$$

$$\frac{1}{\lambda_i} = \frac{1}{\lambda + 0.08\beta} + \frac{0.035}{\beta^3 + 1}, \tag{2.7}$$

has $C_p(\lambda,\beta)$ and P_m at different wind speeds as $\beta = 0$ as shown in Fig.2.2. From Fig.2.2a, we can see that at a constant β, $C_p(\lambda)$ has an unique maximum point respecting to λ. At a constant λ, when β increases the $C_p(\beta)$ decreases. Fig.2.2b shows the mechanical power P_m versus ω_r as $\beta = 0$. Obviously, Fig.2.2b can be divided into three regions:

- Parking region

  When the wind speed is below cut-in speed $V_{w-cut-in}$, the wind turbine is locked and the wind turbine system does not operate.

  When $V_w = V_{w-cut-in}$, the wind turbine begins the star-up process. Since the kinetic energy from the wind is insignificant, the wind turbine is controlled at constant speed until the wind speed is equal to a minimum speed $V_{w\,\min}$. This period, $V_{w-cut-in} \leq V_w \leq V_{w\min}$, is considered as the start-up interval of the wind turbine.

- Optimal power control region

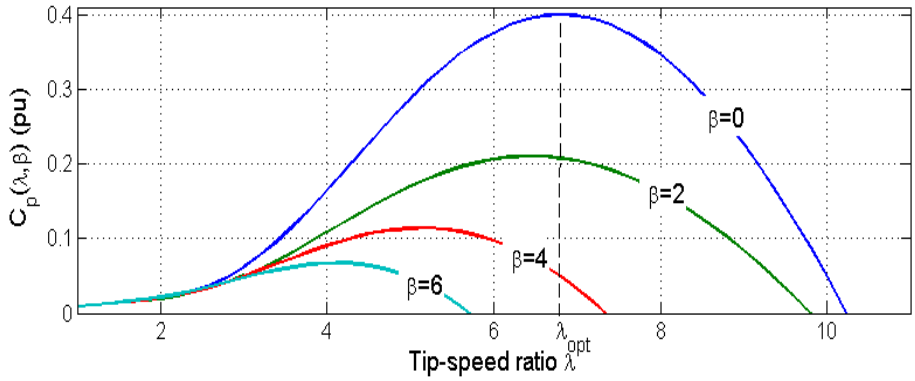

(a)

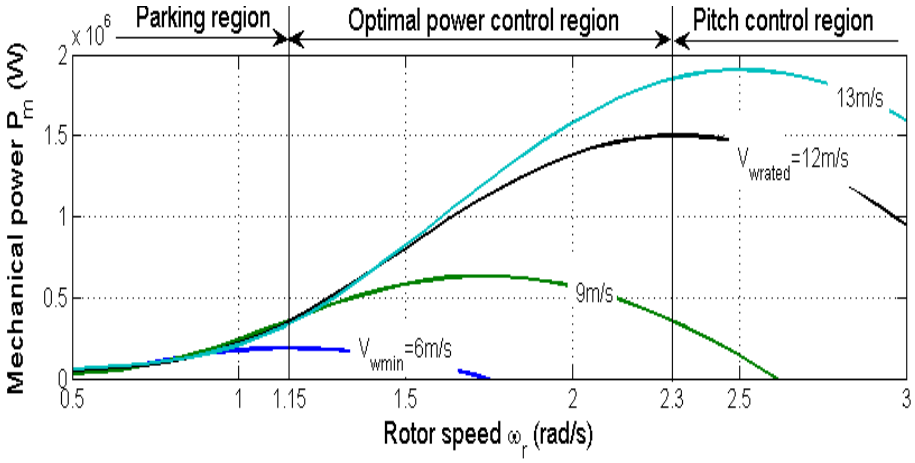

(b)

Fig. 2.2: Characteristic of wind turbine: (a) C_p versus λ and (b) P_m versus ω_r at different wind speeds as $\beta = 0$.

When the wind speed is between $V_{w\min}$ and the rated speed $V_{w\text{rated}}$, $V_{w\min} \leq V_w \leq V_{w\text{rated}}$, the P_m (2.4) always fails to be over its rated value, even though C_p is maximum value. Therefore, to utilize the wind energy optimally, the power coefficient of the wind turbine C_p should be maximum; it means the P_m is maximum. Hence, when the wind turbine operates in the region of $V_{w\min} \leq V_w \leq V_{w\text{rated}}$, the wind turbine is controlled to extract optimal power and this region is called optimal power control region.

From Fig. 2.2a, to get maximum C_p, the pitch angle β should be keep at zero and the wind turbine speed should be adjusted so that λ approaches λ_{opt}. This makes $C_p(\lambda, 0)$ to reache maximum value and then the P_m approaches its maximum value.

- Pitch control region

  When the wind speed is over the rated speed $V_{w\text{rated}} = 12\text{m/s}$, the P_m is over the rated value and this is very dangerous to all equipments in the wind turbine system. In this case, the wind turbine must be controlled to reduce $C_p(\lambda,\beta)$ and as a result, the P_m can be limited at the rated value. From Fig. 2.2a, to decrease $C_p(\lambda,\beta)$, we must increase pitch angle β. Hence, when the wind turbine operates in the region of $V_w > V_{w\text{rated}}$, the pitch system has to be controlled and this region is called pitch contrl region.

This research, we propose two independent methods such that the wind turbine extracts maximum mechanical power as $V_{w\,\min} \le V_w \le V_{w\text{rated}}$. Hence, throughout this paper, we fix β as a constant and we simply denote it as $C_p(\lambda)$.

From (2.3), we can regard P_m as

$$P_m(\omega_r, V_w) = \frac{1}{2}\rho\pi R^2 C_p(\lambda(\omega_r, V_w))V_w^3. \tag{2.8}$$

2.2 DFIG

In the dq frame, the DFIG can be described as [25, 26]

$$\begin{cases} \mathbf{v}_s(t) = R_s\mathbf{i}_s(t) + L_s\frac{d}{dt}\mathbf{i}_s(t) + L_m\frac{d}{dt}\mathbf{i}_r(t) + \omega_s\mathbf{\Theta}(L_s\mathbf{i}_s(t) + L_m\mathbf{i}_r(t)) \\ \mathbf{v}_r(t) = R_r\mathbf{i}_r(t) + L_r\frac{d}{dt}\mathbf{i}_r(t) + L_m\frac{d}{dt}\mathbf{i}_s(t) + \omega_s s(t)\mathbf{\Theta}(L_m\mathbf{i}_s(t) + L_r\mathbf{i}_r(t)) \end{cases} \tag{2.9}$$

where $\mathbf{v}_s = \begin{bmatrix} v_{sd} & v_{sq} \end{bmatrix}^\top$ is the stator-side voltage, $\mathbf{v}_r = \begin{bmatrix} v_{rd} & v_{rq} \end{bmatrix}^\top$ is the rotor-side voltage, $\mathbf{i}_s = \begin{bmatrix} i_{sd} & i_{sq} \end{bmatrix}^\top$ is the stator-side current, $\mathbf{i}_r = \begin{bmatrix} i_{rd} & i_{rq} \end{bmatrix}^\top$ is the rotor-side current and $\mathbf{\Theta} = \begin{bmatrix} 0 & -1 \\ 1 & 0 \end{bmatrix}$. ω, R, L and s represent rotational speed, resistance, inductance and rotor slip, respectively; subscripts r, s and m stand for rotor-side, stator-side and magnetization. Note that ω_s is normally constant.

The rotor slip of the DFIG is defined by:

$$s(t) \triangleq 1 - \frac{\omega_r(t)}{\omega_s}. \tag{2.10}$$

Assumption 1. The stator flux is constant, and the d-axis of the dq-frame is oriented with the stator flux vector. Hence,

$$\mathbf{\Psi}_s(t) = \begin{bmatrix} \Psi_{sd}(t) \\ \Psi_{sq}(t) \end{bmatrix} \equiv \begin{bmatrix} \Psi_{sd} \\ 0 \end{bmatrix} = L_s \mathbf{i}_s(t) + L_m \mathbf{i}_r(t). \tag{2.11}$$

Then,

$$L_s \frac{d}{dt}\mathbf{i}_s(t) + L_m \frac{d}{dt}\mathbf{i}_r(t) = 0. \tag{2.12}$$

Moreover, the resistance of the stator winding can be ignored, *i.e.*, $R_s = 0$.

Lemma 1. Under Assumption 1, in a DFIG (2.9), the stator-side voltage becomes constant as

$$\mathbf{v}_s(t) = \begin{bmatrix} 0 & V_s \end{bmatrix}^\top, \tag{2.13}$$

where V_s is the magnitude of the stator voltage $\|\mathbf{v}_s(t)\|$. Moreover, the rotor-side current $\mathbf{i}_r$ and voltage $\mathbf{v}_r$ satisfy

$$\frac{d}{dt}\mathbf{i}_r(t) = \mathbf{A}_i(t)\mathbf{i}_r(t) + \sigma^{-1}\mathbf{v}_r(t) + \mathbf{d}_i(t), \tag{2.14}$$

where

$$\sigma \triangleq L_r - \frac{L_m^2}{L_s}, \tag{2.15}$$

$$\mathbf{A}_i(t) \triangleq \begin{bmatrix} -\sigma^{-1}R_r & \omega_s s(t) \\ -\omega_s s(t) & -\sigma^{-1}R_r \end{bmatrix}, \tag{2.16}$$

$$\mathbf{d}_i(t) \triangleq -\frac{L_m}{L_s\sigma} s(t) \begin{bmatrix} 0 \\ V_s \end{bmatrix}. \tag{2.17}$$

Proof. By substituting (2.12) and $R_s = 0$ into (2.9), we have (2.13) as

$$\mathbf{v}_s(t) = \begin{bmatrix} 0 \\ \omega_s \Psi_{sd} \end{bmatrix} = \begin{bmatrix} 0 \\ V_s \end{bmatrix}, \tag{2.18}$$

because $V_s = \|\mathbf{v}_s(t)\| = |\omega_s \Psi_{sd}|$. From (2.11) and (2.18), we have

$$L_s \mathbf{i}_s(t) + L_m \mathbf{i}_r(t) = \frac{1}{\omega_s} \begin{bmatrix} V_s \\ 0 \end{bmatrix}. \tag{2.19}$$

Hence,

$$\mathbf{i}_s(t) = -\frac{L_m}{L_s}\mathbf{i}_r(t) + \frac{1}{L_s\omega_s}\begin{bmatrix} V_s \\ 0 \end{bmatrix}, \tag{2.20}$$

$$\frac{d}{dt}\mathbf{i}_s(t) = -\frac{L_m}{L_s}\frac{d}{dt}\mathbf{i}_r(t). \tag{2.21}$$

Substituting (2.20) and (2.21) into the second equation of (2.9), we have

$$\begin{aligned}\mathbf{v}_r(t) = R_r\mathbf{i}_r(t) + \left(L_r - \frac{L_m^2}{L_s}\right)\frac{d}{dt}\mathbf{i}_r(t) + \omega_s s(t)\boldsymbol{\Theta}\frac{L_m}{L_s\omega_s}\begin{bmatrix} V_s \\ 0 \end{bmatrix} \\ + \omega_s s(t)\boldsymbol{\Theta}\left(L_r - \frac{L_m^2}{L_s}\right)\mathbf{i}_r(t).\end{aligned} \tag{2.22}$$

From (2.10) and (2.22), we obtain (2.14). □

The power in the stator side are given as [26]

$$\mathbf{x}_{pq}(t) \triangleq \begin{bmatrix} Q_s(t) \\ P_s(t) \end{bmatrix} = \begin{bmatrix} -i_{sq}(t) & i_{sd}(t) \\ i_{sd}(t) & i_{sq}(t) \end{bmatrix}\begin{bmatrix} v_{sd}(t) \\ v_{sq}(t) \end{bmatrix}. \tag{2.23}$$

By substituting (2.18) and (2.19) into (2.23), we have

$$\mathbf{x}_{pq}(t) = V_s\mathbf{i}_s(t) = -\tilde{V}_s\mathbf{i}_r(t) + \frac{1}{L_s\omega_s}\begin{bmatrix} V_s^2 \\ 0 \end{bmatrix}, \tag{2.24}$$

where $\tilde{V}_s = \dfrac{L_m}{L_s}V_s$. When the power loss in the DFIG can be neglected, the power output of the generator P_e is described by

$$P_e(t) = P_s(t) + P_r(t) = (1 - s(t))\,P_s(t), \tag{2.25}$$

where P_r is the rotor-side active power. Hence,

$$T_e(t) = \frac{P_e(t)}{\omega_r(t)} = \frac{p_n N P_s(t)}{\omega_s} = -\frac{p_n N L_m}{L_s\omega_s}V_s i_{rq}(t), \tag{2.26}$$

where, p_n and N are the number of pole pairs and gearbox ratio, respectively.

Lemma 2. A state-space representation of the active power P_s and the reactive power Q_s on the stator side is given by

$$\frac{d}{dt}\mathbf{x}_{pq}(t) = \mathbf{A}_i(t)\mathbf{x}_{pq}(t) - \frac{\tilde{V}_s}{\sigma}\mathbf{v}_r(t) + \mathbf{c}_{pq}(t), \tag{2.27}$$

where

$$\mathbf{c}_{pq}(t) = -\frac{\mathbf{A}_i(t)}{L_s\omega_s}\begin{bmatrix} V_s^2 \\ 0 \end{bmatrix} - \tilde{V}_s\mathbf{d}_i(t) = \frac{V_s^2}{\sigma L_s}\begin{bmatrix} \dfrac{R_r}{\omega_s} \\ L_r s(t) \end{bmatrix}.$$

In addition, under Assumption 1, a state-space representation of the DFIG from (2.9) is described by

$$\frac{d}{dt}\mathbf{x}_{PQ}(t) \quad = \quad \mathbf{A}_{PQ}(t)\mathbf{x}_{PQ}(t) + \mathbf{B}_{PQ}(t)v_r(t) + \mathbf{d}_{PQ}(t), \tag{2.28}$$

where

$$\mathbf{x}_{PQ}(t) = \begin{bmatrix} Q_s(t) \\ P_e(t) \end{bmatrix}, \tag{2.29}$$

$$\mathbf{A}_{PQ}(t) = \mathbf{C}(t)^{-1}\left(\mathbf{A}_i(t)\mathbf{C}(t) - \dot{\mathbf{C}}(t)\right) = \begin{bmatrix} -1 - \dfrac{R_r}{\sigma} & \dfrac{\omega_s^2}{\omega_r(t)}s(t) \\ -\omega_r(t)s(t) & \dfrac{\frac{d}{dt}\omega_r(t) - \omega_s\dfrac{R_r}{\sigma}}{\omega_r(t)} \end{bmatrix}, \tag{2.30}$$

$$\mathbf{B}_{PQ}(t) = -\frac{\tilde{V}_s}{\sigma}\mathbf{C}^{-1}(t), \qquad \mathbf{C}(t) = \begin{bmatrix} 1 & 0 \\ 0 & \dfrac{\omega_s}{\omega_r(t)} \end{bmatrix}, \tag{2.31}$$

$$\mathbf{d}_{PQ}(t) = \mathbf{C}(t)^{-1}\mathbf{c}_{pq}(t) = \frac{V_s^2}{\sigma L_s\omega_s}\begin{bmatrix} R_r \\ L_r\omega_r(t)s(t) \end{bmatrix}. \tag{2.32}$$

Proof. See A.1 for the proof of Lemma 2. □

Chapter 3

Controller Design and Maximum Power Strategy

The main objective of this chapter proposes two new schemes for tracking maximum power point, including improved MPPT scheme and adaptive MPPT scheme, when the wind turbine operates in the optimal power control region. The improved MPPT scheme is independent to the adaptive MPPT scheme. In addition to these schemes, we design two RSC controllers corresponding to these schemes. These RSC controllers are independent together. For the improved MPPT scheme, we design the RSC controller for the power adjustment. For the adaptive MPPT scheme, the RSC controller is designed to adjust the rotor speed and current. Hereafter, following assumptions are used.

Assumption 2. We can measure i_r, i_s, i_g, v_s, and ω_r. In addition, we know parameters R_r, L_s, L_r and L_m and manipulate Q_s, P_e.

Assumption 3. The dq/abc transformation block, the PWM and the IGBT-valves in RSC in Fig.2.1 operate properly.

3.1 Maximum power point tracking

The optimal power control region D of the wind turbine is defined by

$$D \triangleq \{(\omega_r, V_w) \mid \omega_{r\min} \leq \omega_r \leq \omega_{r\text{rated}}, V_{w\min} \leq V_w \leq V_{w\text{rated}}, \text{ and } C_p(\lambda) > 0\}, \quad (3.1)$$

where, $\omega_{r\min}$ and $\omega_{r\text{rated}}$ are the minimum and rated rotor speed; $V_{w\min}$ and $V_{w\text{rated}}$ are the minimum and rated wind speed. In this region, the tip-speed ratio is bounded as

$$\lambda_{\min} \triangleq \frac{R\omega_{r\min}}{V_{w\text{rated}}} \leq \lambda(t) \leq \lambda_{\max} \triangleq \max\{\lambda \mid C_p(\lambda) > 0\}.$$

This research aims to suggest MPPT schemes and controllers such that the wind turbine can work in the optimal power control region D of the MPPT curve.

MPPT-curve method

We consider a maximization of the mechanical power to change ω_r. Evidently, it is equivalent to a maximization of $C_p(\lambda(\omega_r, V_w))$. That is,

$$C_{p\max} \triangleq C_p(\lambda_{\text{opt}}), \tag{3.2}$$

$$\lambda_{\text{opt}} \triangleq \arg\max_{\lambda} C_p(\lambda). \tag{3.3}$$

In this research, we use

$$C_p(\lambda) = \left(165.2842\lambda^{-1} - 16.8693\right) e^{-21\lambda^{-1}} + 0.009\lambda \tag{3.4}$$

for the pitch angle $\beta = 0$. It has an unique maximum point of $C_{p\max} = 0.4$ at $\lambda_{\text{opt}} = 6.7562$, as shown in Fig.3.1a.

The optimal rotor speed

$$\omega_{\text{opt}}(V_w) \triangleq \frac{\lambda_{\text{opt}} V_w}{R}, \tag{3.5}$$

achieves the maximal mechanical power

$$\max_{\omega_r} P_m(\omega_r, V_w) = \frac{1}{2}\rho\pi R^2 C_{p\max} V_w^3 = k_{\text{opt}}\omega_{\text{opt}}^3(V_w), \tag{3.6}$$

$$k_{\text{opt}} \triangleq \frac{1}{2}\rho\pi R^5 \frac{C_{p\max}}{\lambda_{\text{opt}}^3}. \tag{3.7}$$

To maximize the mechanical power, if we have a wind speed V_w, we simply control to make $\omega_r(t)$ track the $\omega_{\text{opt}}(V_w(t))$ given in (3.5). However, since it is difficult to obtain precise values of V_w, we generally control ω_r or P_e to make the mechanical power $P_m(\omega_r, V_w)$ track

$$P_{\text{mppt}}(\omega_r) = k_{\text{opt}}\omega_r^3, \tag{3.8}$$

instead of (3.6). $P_{\text{mppt}}(\omega_r)$ is a locus of the peak of $P_m(\omega_r, V_m)$ as V_m changes in the optimal power control region D Fig.3.1b. This is called the MPPT-curve method or MPPT scheme.

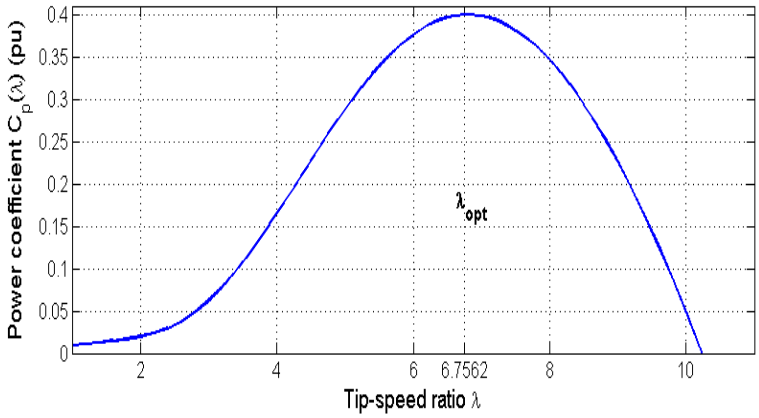

(a)

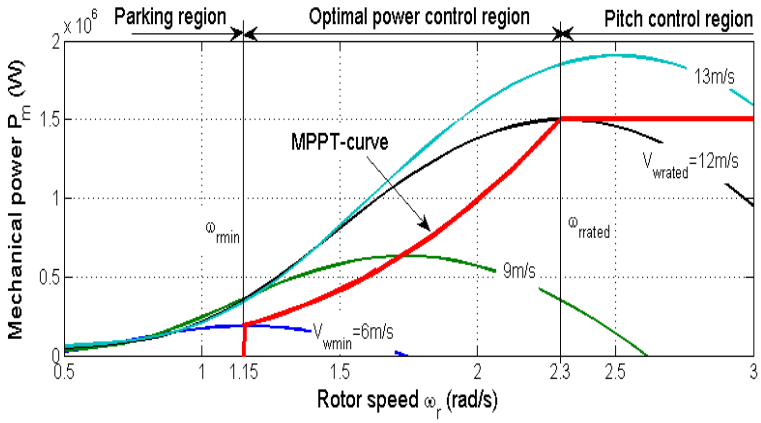

(b)

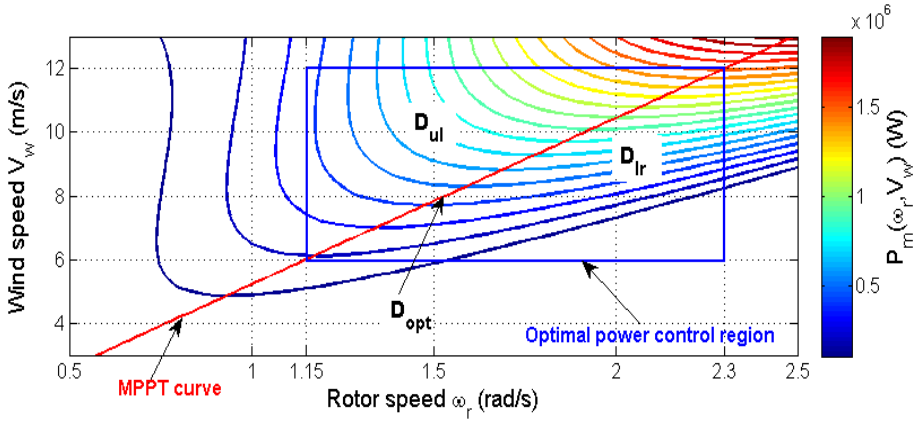

(c)

Fig. 3.1: Wind turbine characteristic of (3.4) for $\beta = 0$: (a) $C_p(\lambda)$, (b) $P_m(\lambda, V_w)$ and $P_{\text{mppt}}(\omega_r)$, and (c) contour of wind turbine.

Note that the optimal control region D is divided into three parts as Fig. 3.1c

$$D_{\mathrm{lr}} \triangleq \left\{(\omega_r, V_w) \in D \mid R\omega_r/V_w > \lambda_{\mathrm{opt}}\right\} \tag{3.9}$$

$$D_{\mathrm{opt}} \triangleq \left\{(\omega_r, V_w) \in D \mid R\omega_r/V_w = \lambda_{\mathrm{opt}}\right\} \tag{3.10}$$

$$D_{\mathrm{ul}} \triangleq \left\{(\omega_r, V_w) \in D \mid R\omega_r/V_w < \lambda_{\mathrm{opt}}\right\}. \tag{3.11}$$

Moreover, from Fig. 3.1a and Fig. 3.1c, we have

$$\frac{\partial}{\partial\lambda}C_p(\lambda)\begin{cases} < 0 & (\omega_r, V_w) \in D_{\mathrm{lr}} \\ = 0 & (\omega_r, V_w) \in D_{\mathrm{opt}} \\ > 0 & (\omega_r, V_w) \in D_{\mathrm{ul}}. \end{cases} \tag{3.12}$$

In the analysis of the proposed scheme, we use

$$\zeta(\omega_r, V_w) \triangleq -\frac{P_m(\omega_r, V_w) - P_{\mathrm{mppt}}(\omega_r)}{\omega_r(\omega_r - \omega_{r\mathrm{opt}}(V_w))}. \tag{3.13}$$

By using L'Hôpital's rule, we ensure that

$$\begin{aligned}\lim_{\omega_r\to\omega_{r\mathrm{opt}}(V_w)}\zeta(\omega_r, V_w) &= -\lim_{\omega_r\to\omega_{r\mathrm{opt}}(V_w)}\frac{\dfrac{\mathrm{d}}{\mathrm{d}\omega_r}P_m(\omega_r, V_w) - \dfrac{\mathrm{d}}{\mathrm{d}\omega_r}P_{\mathrm{mppt}}(\omega_r)}{\dfrac{\mathrm{d}}{\mathrm{d}\omega_r}(\omega_r(\omega_r - \omega_{r\mathrm{opt}}(V_w)))} \\ &= -\lim_{\omega_r\to\omega_{r\mathrm{opt}}(V_w)}\frac{\dfrac{R}{V_w}\dfrac{\partial}{\partial\lambda}P_m(\lambda, V_w) - 3k_{\mathrm{opt}}\omega_r^2}{2\omega_r - \omega_{r\mathrm{opt}}(V_w)} \\ &= \frac{3k_{\mathrm{opt}}\omega_{r\mathrm{opt}}(V_w)^2}{\omega_{r\mathrm{opt}}(V_w)} = 3k_{\mathrm{opt}}\omega_{r\mathrm{opt}}(V_w).\end{aligned} \tag{3.14}$$

By regarding (2.8) to use (2.3) as

$$P_m(\omega_r, \lambda) = \frac{1}{2}\rho\pi R^5\frac{C_p(\lambda)}{\lambda^3}\omega_r^3 \tag{3.15}$$

and from $P_{\mathrm{mppt}}(\omega_r) = k_{\mathrm{opt}}\omega_r^3$ and the definition of k_{opt} in (3.7), we have

$$P_m(\omega_r, V_w) - P_{\mathrm{mppt}}(\omega_r) = \frac{1}{2}\rho\pi R^5\omega_r^3\left(\frac{C_p(\lambda)}{\lambda^3} - \frac{C_{p\max}}{\lambda_{\mathrm{opt}}^3}\right). \tag{3.16}$$

Hence,

$$\zeta(\omega_r, V_w) = \frac{\rho\pi R^5\omega_r^2}{2(\omega_r - \omega_{r\mathrm{opt}}(V_w))}\left(\frac{C_{p\max}}{\lambda_{\mathrm{opt}}^3} - \frac{C_p(\lambda)}{\lambda^3}\right) \tag{3.17}$$

$$= \frac{\rho\pi R^6\omega_r^2}{2V_w\lambda^3(\lambda - \lambda_{\mathrm{opt}})}\left(\frac{C_{p\max}}{\lambda_{\mathrm{opt}}^3}\lambda^3 - C_p(\lambda)\right). \tag{3.18}$$

Lemma 3. For a point $(\omega_r, V_w) \in D_{\text{opt}} \cup D_{\text{lr}}$, $\zeta(\omega_r, V_w) > 0$. Moreover, for a point $(\omega_r, V_w) \in D_{\text{ul}}$, if

$$\frac{C_{p\max}}{\lambda_{\text{opt}}^3} - \frac{C_p(\lambda)}{\lambda^3} < 0, \tag{3.19}$$

then

$$\zeta(\omega_r, V_w) > 0. \tag{3.20}$$

Proof. See B.1 for the proof of Lemma 3. □

Remark 1. From (3.8) and (3.13), we can write

$$P_m(t) - k_{\text{opt}}\omega_r^3(t) = -\zeta_p(V_w, \omega_r)\left(\lambda(t) - \lambda_{\text{opt}}\right), \tag{3.21}$$

where

$$\zeta_p(V_w, \omega_r) = \zeta(V_w, \omega_r)\frac{V_w(t)\omega_r(t)}{R}, \tag{3.22}$$

and $\zeta_p(V_w, \omega_r)$ is also positive, continuous and bounded in the region D.

Assumption 4. When the wind turbine operates in the region D,

$$\left|\frac{d}{dt}\omega_{r\text{opt}}(V_w(t))\right| = \frac{\lambda_{\text{opt}}}{R}\frac{d}{dt}V_w(t) \leq \frac{\lambda_{\text{opt}}}{R}\left|\frac{d}{dt}V_w(t)\right| \triangleq \gamma. \tag{3.23}$$

3.2 Design RSC controller for improved MPPT scheme

This section, we will design a control law for the RSC to adjust the power output of the DFIG and an improved MPPT method which develop from the MPPT-curve method.

3.2.1 RSC Controller for power adjustment

The objective of RSC is to maintain, at the desired references, the reactive power in the stator side Q_s and the total active power output P_e of the DFIG,

$$\mathbf{x}_{\text{r}}^{\top} = \begin{bmatrix} Q_{s\text{ref}} & P_{e\text{ref}} \end{bmatrix}^{\top}. \tag{3.24}$$

From (2.28), to adjust Q_s and P_e, v_{rd} and v_{rq} must be regulated, respectively. To perform this task, previous studies employed PI controllers [12, 27]. Hereafter, a new control law is proposed.

Lemma 4. Under Assumptions 1 and 2, when we can measure $\frac{d}{dt}\omega_r(t)$ for any desired reference $\mathbf{x}_\mathrm{r}$ from (3.24), if we use any positive definite matrix $\mathbf{P}$,

$$\mathbf{v}_r(t) = -\mathbf{B}_{PQ}(t)^{-1}\left(\mathbf{A}_{PQ}(t)\mathbf{x}_{PQ}(t) + \mathbf{P}(\mathbf{x}_r(t) - \mathbf{x}_{PQ}(t)) - \frac{d}{dt}\mathbf{x}_\mathrm{r}(t) + \mathbf{d}_{PQ}(t)\right) \tag{3.25}$$

for the DFIG (2.28), then it is ensured that

$$\lim_{t\to\infty}(\mathbf{x}_r(t) - \mathbf{x}_{PQ}(t)) = 0. \tag{3.26}$$

Proof. See B.2 for the froof of Lemma 4. □

From Lemma 4, if the rotor voltage $\mathbf{v}_r$ is designed as (3.25), the power output of DFIG will converge to its reference value given by (3.24).

3.2.2 Improved MPPT scheme

The main objective of this subsection is to propose a new MPPT scheme that improves the conventional MPPT-curve method [12] so that P_m approaches the neighbor of P_max as $\omega_{r\mathrm{min}} \le \omega_r(t) < \omega_{r\mathrm{rated}}$. From (3.5) and (3.6), $P_m(t)$ only reaches the neighbor of P_max as ω_r approaches the neighbor of $\omega_{r\mathrm{opt}}$ or λ approaches the neighbor of λ_opt. Therefore, in this subsection, a new strategy is proposed, such that λ approaches the neighbor of λ_opt.

Theorem 1. Under Assumption 4, suppose that we use a positive constant $\alpha < J$, k_opt in (3.7), and $P_{e\mathrm{ref}}$ in (3.24) for the RSC control (3.25) as

$$P_{e\mathrm{ref}}(t) \;=\; k_\mathrm{opt}\omega_r^3(t) - \alpha\omega_r(t)\frac{d}{dt}\omega_r(t), \tag{3.27}$$

if there exists a positive constant χ, such that

$$\tilde{\mathbf{P}} := 2\mathbf{P} - \begin{bmatrix} 0 & 0 \\ 0 & \chi^{-1}\dfrac{\lambda(t)}{(J-\alpha)\omega_r^2(t)} \end{bmatrix} > 0 \tag{3.28}$$

for the definite matrix $\mathbf{P} > 0$ in (3.25) and all t, then there exists a time $t_0 > 0$, such that

$$\left|\lambda(t) - \lambda_\mathrm{opt}\right| \;\le\; 2(J-\alpha)\gamma\frac{R}{\lambda_\mathrm{opt}}\max\frac{\omega_r^2(t)}{(2\zeta_p(t) - \chi)V_w(t)}, \tag{3.29}$$

for all $t \ge t_0$.

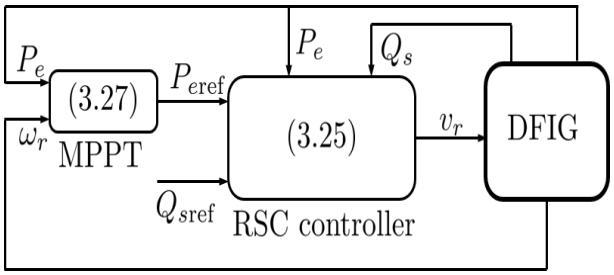

Fig. 3.2: Control diagram using the improved MPPT method.

Proof. See B.3 for the proof of Theorem 1. □

From Theorem 1, if the reference power $P_{e\text{ref}}$ in (3.24) is calculated as (3.27), the tip-speed ratio λ of the wind turbine will converge to the neighbor of λ_{opt} and, hence, P_m will approach its maximum value. Hence, we have control diagram as Fig. 3.2.

Remark 2. By multiplying two side of (3.29) by $\frac{V_w}{R}$, we have

$$\left|\omega_r(t) - \omega_{ropt}(t)\right| = \left|\lambda(t) - \lambda_{\text{opt}}\right| \frac{V_w}{R} \leq 2(J-\alpha)\gamma \frac{V_{w\text{rated}}}{\lambda_{\text{opt}}} \max \frac{\omega_r^2(t)}{(2\zeta_p(t) - \chi)V_w(t)}. \tag{3.30}$$

3.3 Design RSC controller for adaptive MPPT scheme

In this section, I will propose a new control law for the RSC to adjust the rotor speed and a new MPPT method which is named adaptive MPPT scheme. Noted that the RSC controller and adaptive MPPT scheme in this section are independent to the RSC controller and improved MPPT scheme which were designed in Section 3.2.

3.3.1 RSC controller for rotor speed adjustment

The objective of RSC is to maintain the i_{rd} of the DFIG and the rotor speed ω_r of the wind turbine at the desired references. From (2.1), (2.14), and (2.26), to control i_{rd} and ω_r, we can adjust i_{rd} and i_{rq} by v_{rd} and v_{rq}, respectively. To achieve this task, in previous research, traditional PI control was used [12, 28, 29, 30, 31]. In this research, a new law for rotor speed control is proposed.

Lemma 5. Under Assumptions 2 and 3, for any reference $i_{rd\text{ref}}$ and $\omega_{r\text{ref}}$, if $\mathbf{v}_r$ of the DFIG (2.9) is designed as

$$\mathbf{v}_r(t) = \sigma(-\mathbf{A}_i(t)\mathbf{i}_r(t) - \mathbf{d}_i(t) + \frac{d}{dt}\mathbf{i}_{r\text{ref}}(t) + \mathbf{K}\left(\mathbf{i}_{r\text{ref}}(t) - \mathbf{i}_r(t)\right)), \tag{3.31}$$

where, for $k_d > 0$,

$$\mathbf{i}_{r\text{ref}}(t) \triangleq \begin{bmatrix} i_{rd\text{ref}}(t) \\ i_{rq\text{ref}}(t) \end{bmatrix} = \begin{bmatrix} i_{rd\text{ref}}(t) \\ i_{rq}(t) + k_d \frac{d}{dt}(\omega_{r\text{ref}}(t) - \omega_r(t)) + k_p(\omega_{r\text{ref}}(t) - \omega_r(t)) \end{bmatrix}, \tag{3.32}$$

and if the feedback gain $\mathbf{K}$ and k_p satisfy

$$\tilde{\mathbf{Q}} \triangleq \begin{bmatrix} 2k_p & \begin{bmatrix} 0 & -1 \end{bmatrix} \\ \begin{bmatrix} 0 \\ -1 \end{bmatrix} & \mathbf{K}^\top + \mathbf{K} \end{bmatrix} > 0, \tag{3.33}$$

then

$$\lim_{t\to\infty}\left(\mathbf{i}_{r\text{ref}}(t) - \mathbf{i}_r(t)\right) = 0, \text{ and } \lim_{t\to\infty}\left(\omega_{r\text{ref}}(t) - \omega_r(t)\right) = 0. \tag{3.34}$$

Proof. See B.4 for the proof of Lemma 5. □

Hence, from Lemma 5 and Assumption 3, if the rotor-side voltage of the DFIG is adjusted to satisfy (3.31), $\mathbf{i}_r(t)$ and $\omega_r(t)$ will converge to the desired values $\mathbf{i}_{r\text{ref}}(t)$ and $\omega_{r\text{ref}}(t)$, respectively.

3.3.2 Adaptive MPPT scheme

In this subsection, we propose a new MPPT scheme using no real-time information about $V_w(t)$. The scheme aims to reduce $|\omega_{r\text{opt}}(V_w(t)) - \omega_r(t)|$ to achieve the maximum $P(\omega_r, V_w)$.

Assumption 5. The precise value of k_{opt} for the MPPT curve is not available. Instead, we can use the estimate k'_{opt} with

$$k'_{\text{opt}} = (1 + \delta)k_{\text{opt}}, \quad |\delta| \le \delta_{\max}. \tag{3.35}$$

The proposed MPPT scheme is given as the reference $\omega_{r\text{ref}}$ in (3.32) for the RSC control (3.31) as

$$\omega_{r\text{ref}}(t) \triangleq \left(\frac{\hat{P}_{\text{mppt}}(t)}{\hat{k}_{\text{opt}}(t)}\right)^{1/3}, \tag{3.36}$$

$$\hat{P}_{\text{mppt}}(t) = \omega_r(t)\left(k_1\frac{d}{dt}\omega_r(t) - k_2\left(\omega_r(t) - \hat{\omega}_{r\text{opt}}(t)\right)\right) + P_e(t), \tag{3.37}$$

$$\frac{d}{dt}\hat{\omega}_{r\text{opt}}(t) \triangleq k_3\left(\omega_r(t) - \hat{\omega}_{r\text{opt}}(t)\right), \tag{3.38}$$

$$\frac{d}{dt}\hat{k}_{\text{opt}}(t) \triangleq k_4(k'_{\text{opt}} - \hat{k}_{\text{opt}}(t)) + \omega_r(t)^2\left(\omega_r(t) - \hat{\omega}_{r\text{opt}}(t)\right), \tag{3.39}$$

where $\hat{k}_{\text{opt}}(t)$ and $\hat{\omega}_{r\text{opt}}(t)$ are estimations of k_{opt} and $\omega_{r\text{opt}}(V_w(t))$, respectively. The feedback gains k_1, k_2, k_3, and k_4 are designed as the conditions in Theorem 2 and

$$J > k_1 \geq 0. \tag{3.40}$$

Lemma 6. In the optimal power control region D, $\hat{k}_{\text{opt}}(t)$ is bounded, i.e.,

$$\max \hat{k}_{\text{opt}}(t) \leq \hat{k}_{\text{opt,ub}}, \tag{3.41}$$

$$\hat{k}_{\text{opt,ub}} = 2k_4^{-1}\omega_{r\text{rated}}^3 + k_4^{-1}\left|\hat{\omega}_{r\text{opt}}(0)\right|\omega_{r\text{rated}}^2 + \left|\hat{k}_{\text{opt}}(0)\right| + k'_{\text{opt}}. \tag{3.42}$$

Proof. See B.6 for the proof of Lemma 6. □

Theorem 2. In addition to Assumption 5, we suppose that $\omega_{r\text{ref}}$ (3.36) for the RSC control (3.31)-(3.32) is restricted within the optimal control region D as

$$(\omega_{r\text{ref}}(t), V_w) \in D, \tag{3.43}$$

if there exist positive constants α, v, w and q satisfying

$$\begin{cases} \boldsymbol{\Xi} = \mathbf{K}^\top + \mathbf{K} - q\mathbf{I}_2 > 0, \\ 2k_p - \alpha\hat{k}_{\text{opt,ub}}^2\xi_{\max}^2 - \begin{bmatrix} 0 & 1 \end{bmatrix}\boldsymbol{\Xi}^{-1}\begin{bmatrix} 0 \\ 1 \end{bmatrix} - qk_d > 0, \\ 2\zeta_{\min} - (w\gamma + q)\hat{J} - (k_3 - k_2) - 1 > 0, \\ k_3 - k_2 - \omega_{r\text{rated}}^2 - w\gamma - q > 0, \\ (2 - vk_{\text{opt}})k_4 - \omega_{r\text{rated}}^2 - q > 0, \end{cases} \tag{3.44}$$

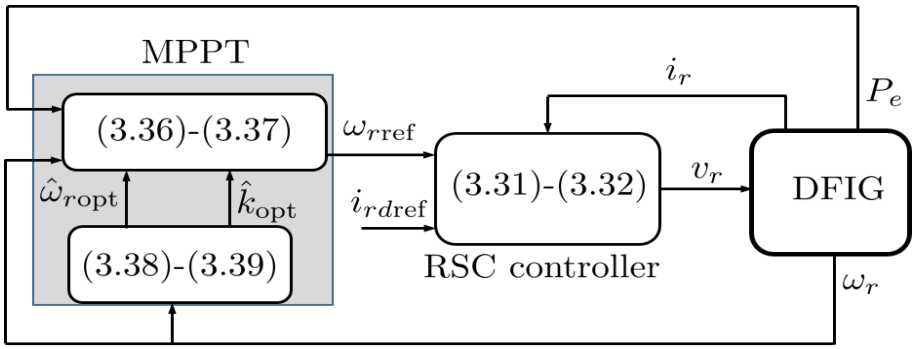

Fig. 3.3: Control diagram using the adaptive MPPT method.

where

$$\zeta_{\min} \triangleq \min \zeta(\omega_r, V_w), \tag{3.45}$$

$$\xi(\omega_r, \omega_{r\text{ref}}) \triangleq \omega_r^{-1}\omega_{r\text{ref}}^2 + \omega_r + \omega_{r\text{ref}}, \tag{3.46}$$

$$\xi_{\max} \triangleq \max \xi(\omega_r, \omega_{r\text{ref}}), \tag{3.47}$$

$$\hat{J} \triangleq J - k_1 > 0, \tag{3.48}$$

then, there exists a time $t_o > 0$ such that for all $t \geq t_o$,

$$\left|\omega_r(t) - \omega_{r\text{opt}}(V_w(t))\right| < \frac{1}{\sqrt{q}}\sqrt{\frac{1+\hat{J}^{-1}}{w}\gamma + \frac{k_4\hat{J}^{-1}}{v}k_{\text{opt}}\delta_{\max}^2}. \tag{3.49}$$

Proof. See B.7 for the proof of Theorem 2. □

From Theorem 2, if the reference rotor speed $\omega_{r\text{ref}}$ for the RSC control (3.31)-(3.32) is designed as (3.36), the rotor speed ω_r of the wind turbine will converge to the neighbor of $\omega_{r\text{opt}}$ and hence, P_m will approach its maximum value. Hence, we have control diagram as Fig.3.3.

3.4 Comparison of two proposed MPPT schemes

In Subsection 3.2.2 and Subsection 3.3.2, we proposed two MPPT schemes independently. The main aim of both two schemes makes the mechanical power P_m of the wind turbine approach its maximum value. Table 3.1 is the comparison of two proposed schemes. From this table, when we do not exactly k_{opt} we must use the

adaptive MPPT method and when we know exactly k_{opt} we can use one of these methods.

Table 3.1: Comparision of two MPPT methods

	Improved MPPT method	Adaptive MPPT method
Main objective	$P_m \rightarrow P_{m\max}$	$P_m \rightarrow P_{m\max}$
Method	Adjust the electric power P_e	Adjust the rotor speed ω_r
Reference signal	$P_{e\text{ref}}$	$\omega_{r\text{ref}}$
Requiring RSC controller	$P_e \rightarrow P_{e\text{ref}}$	$\omega_r \rightarrow \omega_{r\text{ref}}$
Parameter	know k_{opt}	unknow k_{opt}

Chapter 4

Simulation and Discussions

In this chapter, we evaluate the performance of the proposed MPPT schemes by comparing the simulation results for the 1.5 MW DFIG wind turbine with the conventional MPPT-curve method with traditional PI control [12]. In all simulations, we used the parameters of generator [25] and the wind turbine as shown in Table 4.1. We used the power coefficient (3.4) by setting $\beta = 0$. Then,

$$k_{\text{opt}} = 1.2467 \times 10^5 \text{ kg·m}^2, \ \lambda_{\text{opt}} = 6.7562.$$

The optimal control region D is defined by

$$\begin{aligned}
\omega_{r\text{min}} &= 1.15 \text{ rad/s}, \quad \omega_{r\text{rated}} = 2.3 \text{ rad/s}, \\
V_{w\text{min}} &= \frac{R\omega_{r\text{min}}}{\lambda_{\text{opt}}} = \frac{35.25 \times 1.15}{6.7562} = 6 \text{ m/s}, \\
V_{w\text{rated}} &= 12\text{m/s}.
\end{aligned}$$

The wind speed profile Fig.4.2 we used satisfied $V_w(t) < V_{w\text{rated}}$, and $\left|\frac{d}{dt}V_w(t)\right| \leq 0.44$ m/s^2. Hence,

$$\gamma = \frac{\lambda_{\text{opt}} 0.44}{R} = \frac{6.7562 \times 0.44}{35.25} = 0.0843.$$

In D, $\lambda_{\text{max}} = 10.239$ and

$$\lambda_{\text{min}} = \frac{R\omega_{r\text{min}}}{V_{w\text{rated}}} = \frac{35.25 \times 1.15}{12} = 3.4 \text{ p.u.}$$

Table 4.1: Parameters in simulations (DFIG[25] and wind turbine)

Name	Symbol	Value	Unit
Rated power	P	1.5	MW
The length of blade	R	35.25	m
Normal rotor speed	$\omega_{r\text{rated}}$	22	rpm
Minimum rotor speed	$\omega_{r\min}$	11	rpm
Rated wind speed	$V_{w\text{rated}}$	12	m/s
Rated stator voltage	V_s	690	V
Rated rotor voltage	V_r	120	V
Rated stator frequency	f	50	Hz
Minimum rotor speed	$\Omega_{r\,\min}$	1200	rpm
Rated rotor speed	$\Omega_{r\text{rated}}$	1750	rpm
Number of pole pairs	p_n	2	p.u
Stator winding resistance	R_s	2.65	mΩ
Rotor winding resistance	R_r	2.63	mΩ
Stator winding inductance	L_s	5.6438	mH
Rotor winding inductance	L_r	5.6068	mH
Magnetizing inductance	L_m	5.4749	mH
Gearbox ratio	N	79.545	p.u
Inertia of system	J	445000	kg·m^2

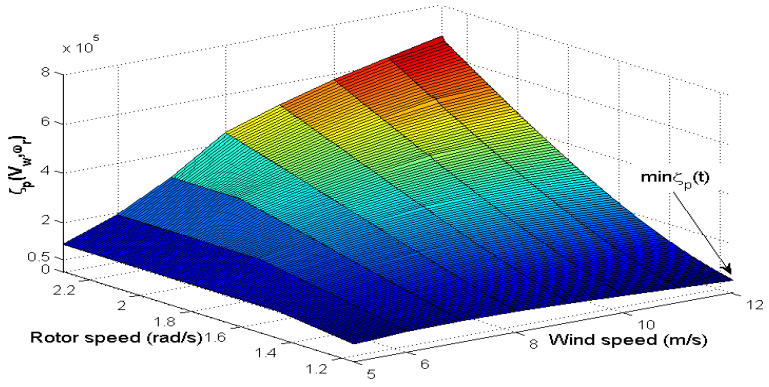

(a)

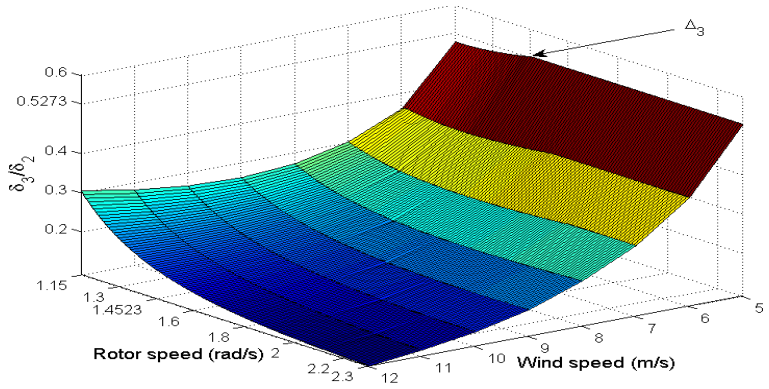

(b)

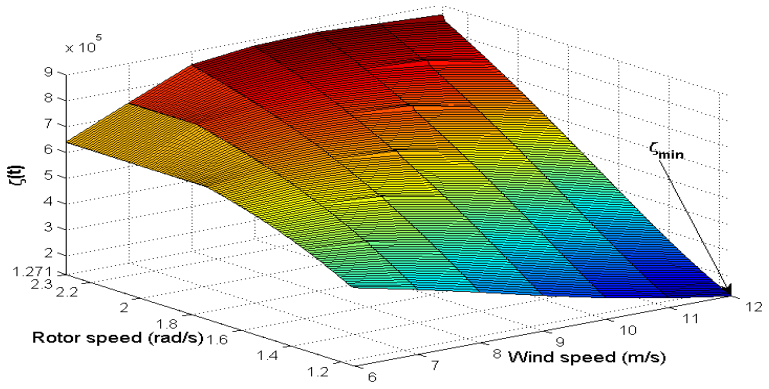

(c)

Fig. 4.1: $\zeta_p(\omega_r, V_w)$ (a), $\dfrac{\delta 3}{\delta 2}$ (b), and $\zeta(\omega_r, V_w)$.

4.1 Parameters for improved MPPT method

The reference value setting for the RSC from (3.25), with $Q_{s\text{ref}}(t) = 0$ are

$$P = \begin{bmatrix} 2 & 0 \\ 0 & 2 \end{bmatrix}. \tag{4.1}$$

We used $P_{e\text{ref}}$ for the RSC control from (3.27) with $\alpha = 0.3J$. We have

$$\max \delta_1(t) = \frac{\lambda_{\max}}{\eta \omega_{r\min}^2} = \frac{13.4}{3.12 \times 10^5 \times 1.15^2} \approx 0 \tag{4.2}$$

where $\eta = J - \alpha = 0.7J = 3.12 \times 10^5 \text{kg} \cdot \text{m}^2$. With $5\text{m/s} \leq V_w(t) \leq 12\text{m/s}$ and $1.15\text{rad/s} \leq \omega_r(t) \leq 2.3\text{rad/s}$, ζ_p *versus* ω_r and V_w are shown in Figure 4.1a. From Figure 4.1a, we can obtain $\min \zeta_p(t) = 0.5 \times 10^5$; we choose $\chi = 1$. With $\chi = 1$, $\frac{\delta_3}{\delta_2}$ *versus* ω_r and V_w are shown in Figure 4.1b. From that figure, we obtain $\Delta_3 = 0.5273$. Obviously, the condition in (3.33) is satisfied, and (3.29) gives the bound of the tip-speed ratio λ as

$$\begin{aligned} & \left|\lambda(t) - \lambda_{\text{opt}}\right| \leq \Delta_3 = 0.5273, \\ \text{or} \qquad & \left|\omega_r(t) - \omega_{r\text{opt}}\right| \leq \Delta_3 \frac{V_{rated}}{R} = 0.1795\text{rad/s}. \end{aligned}$$

4.2 Parameters for adaptive MPPT method

The reference values setting for the RSC control (3.31) with $i_{rd\text{ref}} = 401.4\text{A}$,

$$\mathbf{K} = 200\mathbf{I}_2.$$

Note that as $i_{rd}(t) \to 401.4$ A, the DFIG will generate with a unity power factor. Here, we used $\omega_{r\text{ref}}(t)$ with

$$\begin{aligned} & k_1 = 0.3J, \hat{J} = J - k_1 = 0.7J = 3.12 \times 10^5, \\ & k_2 = 2\hat{J},\ k_3 = k_2 + 0.001\hat{J},\ k_4 = 10,\ k_d = 0.0029J,\ k_p = 100k_d, \\ & \hat{\omega}_{r\text{opt}}(0) = \omega_{r\text{rated}}, k'_{\text{opt}} = 124610,\ \delta_{\max} = 5k_{\text{opt}} \times 10^{-4}, \\ & \hat{k}_{\text{opt}}(0) = k'_{\text{opt}},\ \hat{k}_{\text{opt,ub}} = k'_{\text{opt}} + k'_{\text{opt}} + 3k_4^{-1}\omega_{r\text{rated}}^3 \approx 2k_{\text{opt}}. \end{aligned}$$

From (3.23) and (3.46), we have

$$\max \xi\left(\omega_r, \omega_{r\text{ref}}\right) = \frac{\omega_{r\text{rated}}^2}{\omega_{r\min}} + \omega_{r\min} + \omega_{r\text{rated}} = \frac{2.3^2}{1.15} + 1.15 + 2.3 = 8.05.$$

Obviously, since the power coefficient (3.4) satisfies the condition (3.19) in Lemma 3, $\zeta(\omega_r, V_w)$ is always positive, as shown in Fig. 4.1c. From this figure,

$$\min_{(\omega_r, V_w)\in D} \zeta(\omega_r, V_w) = 1.271 \times 10^5.$$

Hence, when $v = 0.6 \times 10^{-5}$, $w = 4.825$, $\alpha = k_d \hat{k}_{\text{opt,ub}}^{-2} \xi_{\max}^{-2}$ and $q = 0.4$

$$\boldsymbol{\Xi} = \mathbf{K}^\top + \mathbf{K} - q\mathbf{I}_2 = \text{diag}\left(399.6, 399.6\right) > 0,$$

$$\begin{bmatrix} 0 & 1 \end{bmatrix} \boldsymbol{\Xi}^{-1} \begin{bmatrix} 0 \\ 1 \end{bmatrix} + qk_d = 0.0025 + 0.4k_d \approx 0.4k_d,$$

$$2k_p - \alpha \hat{k}_{\text{opt,ub}}^2 \xi_{\max}^2 - \begin{bmatrix} 0 & 1 \end{bmatrix} \boldsymbol{\Xi}^{-1} \begin{bmatrix} 0 \\ 1 \end{bmatrix} - qk_d \approx 198.6k_d > 0,$$

and

$$\begin{aligned} 2\zeta_{\min} - w\hat{J}\gamma - (k_3 - k_2) - 1 &\approx 2.542 \times 10^5 - 0.105w\hat{J} - 0.001\hat{J} \\ &= (0.8145 - 0.0843w - 0.001)\hat{J} = 0.4068\hat{J} > q\hat{J}, \\ k_3 - k_2 - \omega_{r\text{rated}}^2 - w\gamma &= 0.001\hat{J} - 2.3^2 - 0.0843w \\ &\approx 3.12 \times 10^2 - 5.6967 = 306.3033 > q, \\ (2 - vk_{\text{opt}})k_4 - \omega_{r\text{rated}}^2 &= (2 - v \times 1.2467 \times 10^5)k_2 - 2.3^2 = 6.26 - 5.29 = 0.97 > q. \end{aligned}$$

It is easily observed that the five inequalities in Theorem 2 are satisfied. Hence, the upper bound for the rotor speed $\omega_r(t)$ in Theorem 2 is

$$\begin{aligned} |\omega_r(t) - \omega_{r\text{opt}}(V_w(t))| &\le \frac{1}{\sqrt{0.4}} \sqrt{\frac{0.0843}{4.825}\left(1 + \frac{1}{3.12 \times 10^5}\right) + \frac{5 \times 25 \times 10^{-8}}{0.6 \times 10^{-5}} \frac{1.2467 \times 10^5}{3.12 \times 10^5}} \\ &= 0.254\text{rad/s}. \end{aligned}$$

4.3 Simulation results and disscusion

For the above DFIG wind turbine, wind profile, and controllers, the simulation results are shown in Fig. 4.3. Fig. 4.3a argues that with the conventional method, the

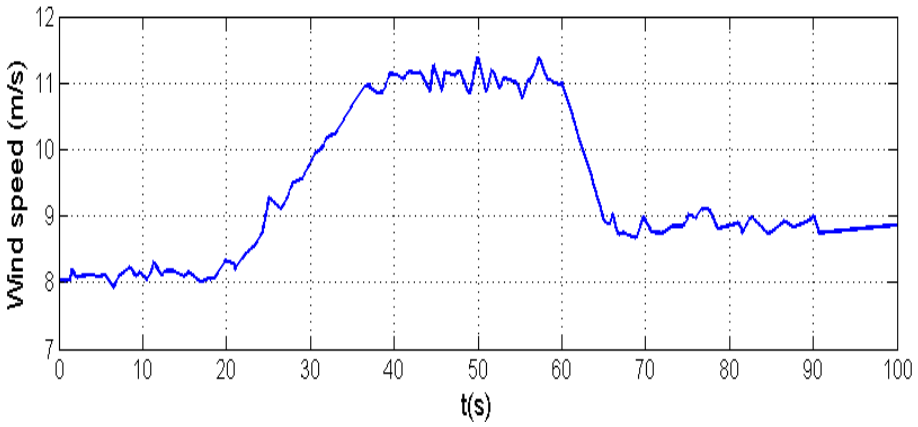

(a)

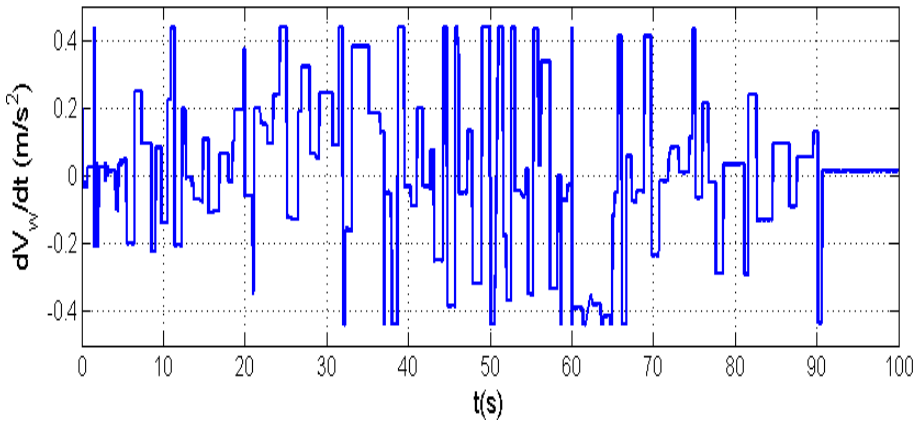

(b)

Fig. 4.2: Wind speed profile: (a) wind speed and (b) wind acceleration.

error between $\omega_r(t)$ and $\omega_{ropt}(t)$ is still quite large, up to 0.3 rad/s. This is unlikely with the proposed methods, as $\omega_r(t)$ always approaches $\omega_{ropt}(t)$ and guarantees that the $|\omega_r(t) - \omega_{ropt}(t)|$ is always very small, below 0.254 rad/s and 0.1795 rad/s, as Theorem 2 and Theorem 1, respectively. Compraring to the case of the improved MPPT method, the adaptive method has a better performance, the maximum of $|\omega_r - \omega_{ropt}(t)|$ is below 0.1 rad/s. Consequently, with the adaptive MPPT method, the power coefficient C_p is virtually maintained around its maximum value $C_{p\max}$= 0.4 p.u. during the simulation interval, as displayed clearly by the blue solid line in Fig. 4.3b. With the improved MPPT method, C_p fails to be maintained around its maximum value $C_{p\max}$= 0.4 p.u. as the wind condition starts to change rappidly but it is retained quickly, as the red discontinueous line inFig.4.3b. This performance is hardly seen in the case with the conventional method, because during the interval

of rapid decrease in the wind speed, the large error in rotor speed, $\omega_r(t) - \omega_{r\text{opt}}(t)$, leads to a reduction of C_p to 0.363 p.u., as shown by the black line in Fig.4.3b.

Concerning the mechanical power output of the wind turbine, Fig.4.3c depicts the error between $P_{\max}$ and P_m. The figure shows that when the wind velocity varies dramatically, the error between $P_{\max}$ and P_m is approximately to zero with the proposed methods, as shown in the blue line and the red broken line. This is mainly because the power coefficient C_p remains around $C_{p\max}$, as shown in Fig.4.3b. In other words, with the proposed methods, the main objective, which is to have P_m approach P_{max}, is completely achieved. With the conventional method, however, this goal is not achievable due to the significant decrease in C_p during sudden variations in wind conditions. Certainly, comparing to the adaptive method, the improved method still gives a bigger error between P_m and $P_{\max}$ during the dramatic change period of the wind.

With the proposed strategies, the total electrical energy output of the generator is higher than that with the conventional strategy, as shown in Fig.4.3d. This is mainly because P_m in the case of the proposed methods has a higher value. This confirms that the quality of the proposed schemes is always better than that of the conventional one.

To evaluate the quality of the RSC controller for the adaptive MPPT method and the improved MPPT method, Fig.4.4 is plotted. Fig.4.4a to Fig.4.4c represent for the adaptive MPPT method while Fig.4.4e stands for the improved MPPT method. Fig.4.4a indicates that during the simulation interval, $\hat{k}_{\text{opt}}$ is always below its maximum value, which is estimated as $\hat{k}_{\text{opt,ub}} = 2k_{\text{opt}}$. From Fig.4.4b, the gap between $\omega_{r\text{opt}}(t)$ and its estimation $\hat{\omega}_{r\text{opt}}(t)$ is quite small, below 0.097rad/s. Fig.4.4b and Fig.4.4c demonstrate that errors, $\omega_{r\text{ref}}(t) - \omega_r(t)$ and $i_{rd\text{ref}}(t) - i_{rd}(t)$, are quite small, approximate to zero, as Lemma 5. Likely, Lemma 4 is guaranteed because the error $x_r(t) - x_{PQ}(t)$ is too small comparing to 1.5MW as Fig.4.4d. In other words, the RSC controllers which designed for the purposes of the adaptive method and the improved method have qualified performance.

To affirm the qualified performance of two proposed schemes, hereafter, two cases of wind speed are used for simulation. Simulation results are shown as Fig.4.5

and Fig.4.6. Obviously, the wind turbine with the proposed methods has better performance than with the conventional one, in terms of both the power coefficient C_p and energy output.

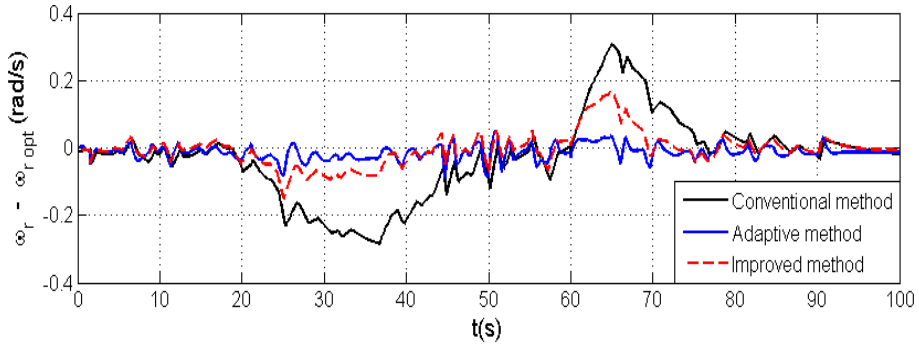

(a)

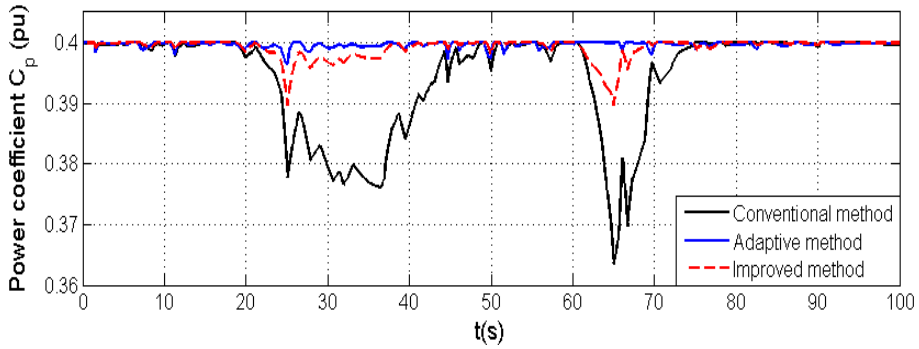

(b)

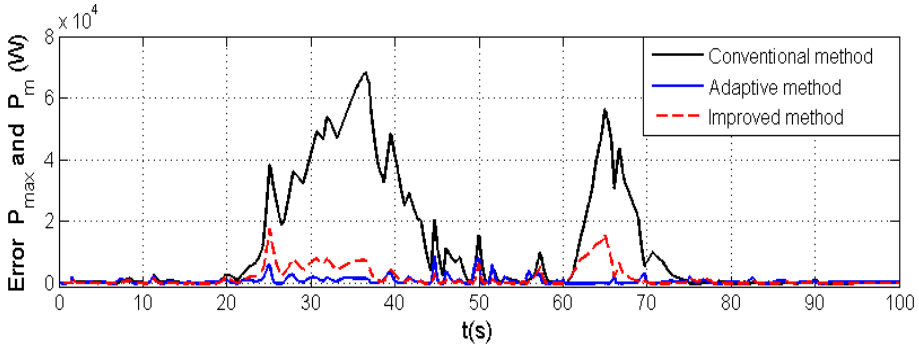

(c)

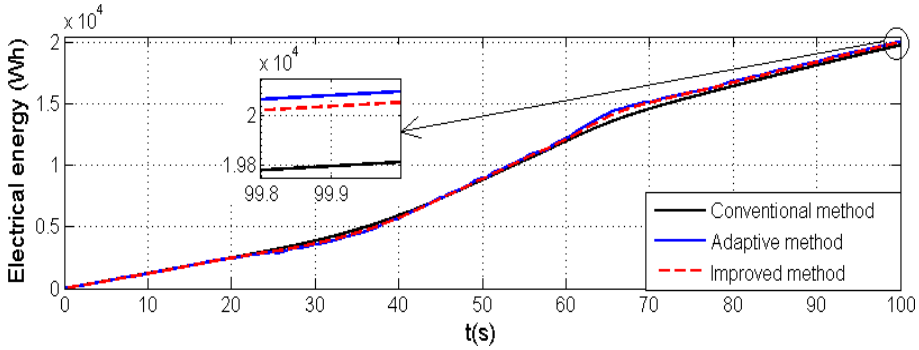

(d)

Fig. 4.3: Simulation results: (a) $\omega_r(t) - \omega_{r\text{opt}}(V_w(t))$, (b) power coefficient $C_p(\lambda(t))$, (c) $P_{\max}(t) - P_m(t)$, and (d) electrical energy output.

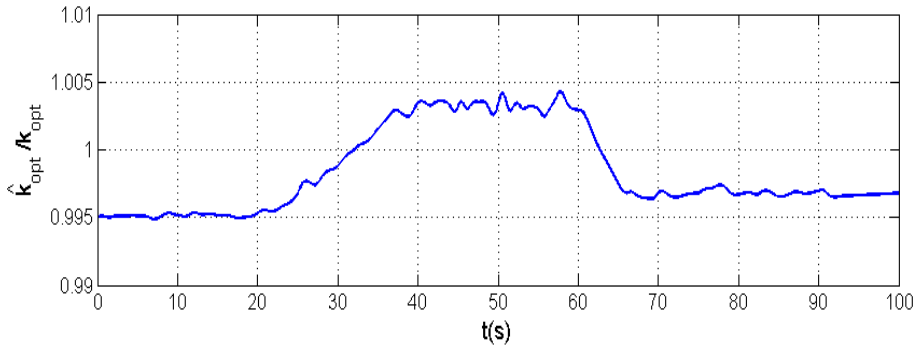

(a)

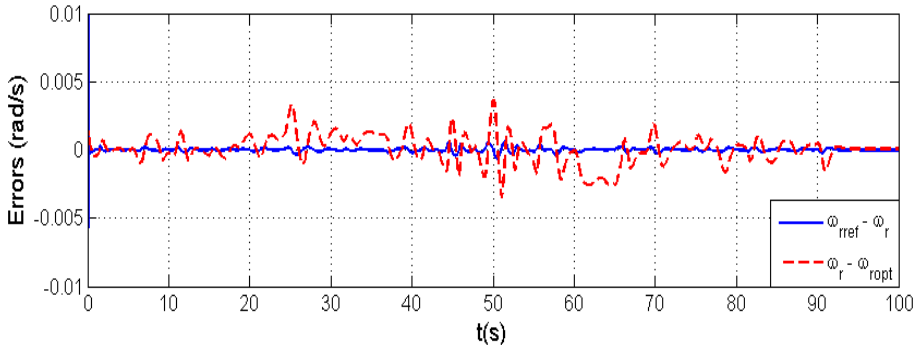

(b)

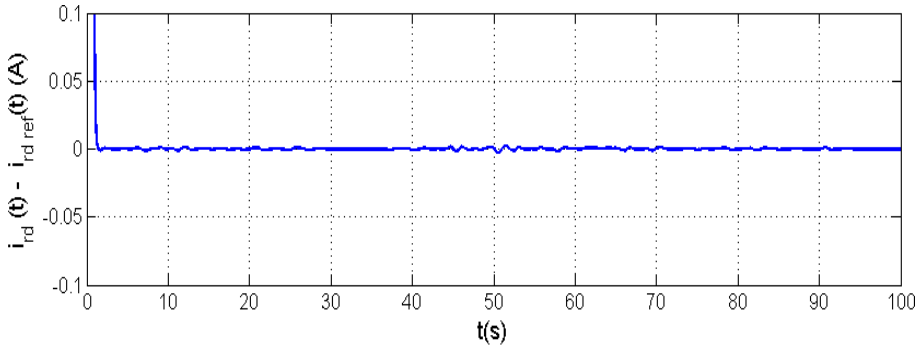

(c)

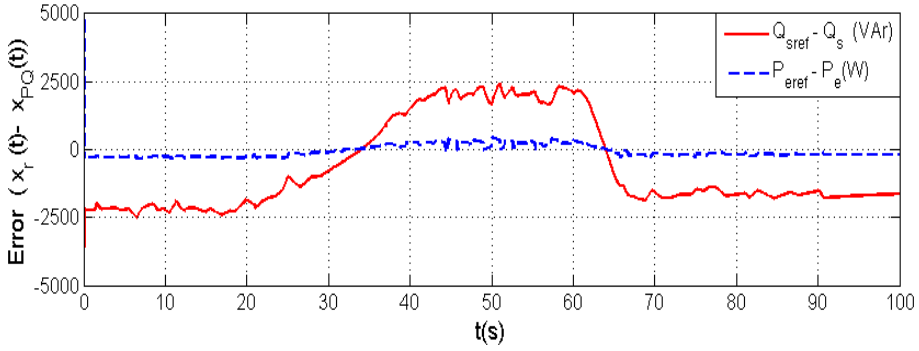

(d)

Fig. 4.4: Simulation results: (a) ratio $\hat{k}_{\text{opt}}/k_{\text{opt}}$ and (b) $\omega_{r\text{opt}}(t) - \hat{\omega}_{r\text{opt}}(t)$, (c) $i_{rd\text{ref}}(t) - i_{rd}(t)$, (d) $x_r(t) - x_{PQ}(t)$.

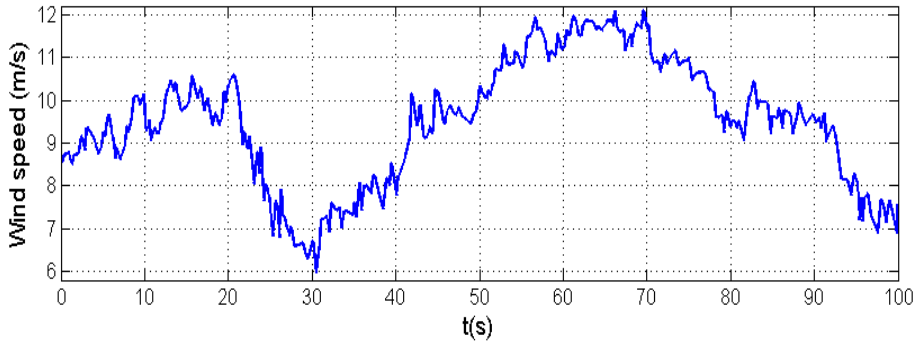

(a)

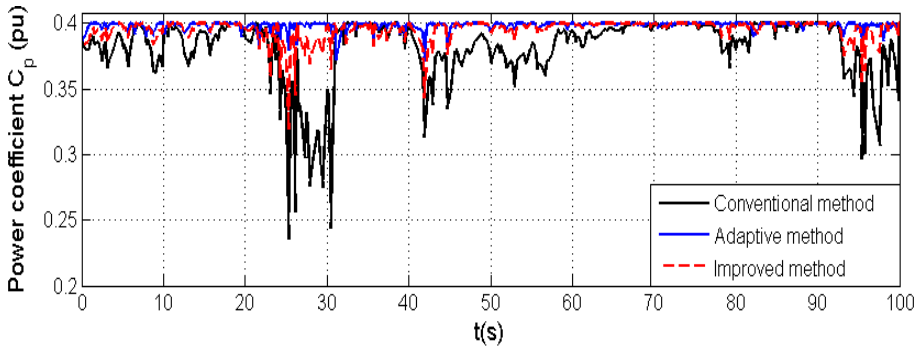

(b)

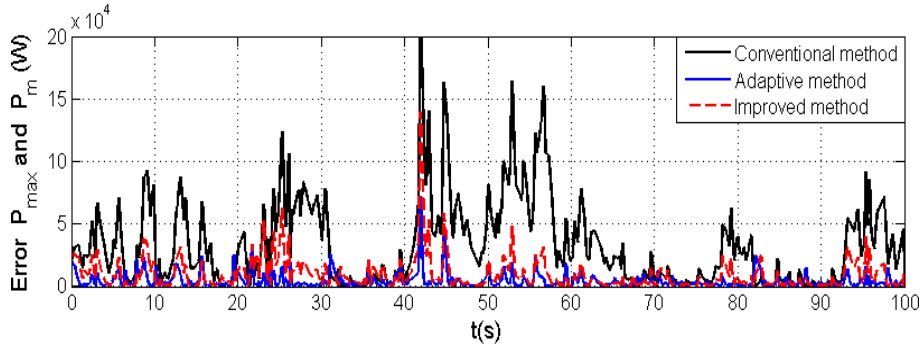

(c)

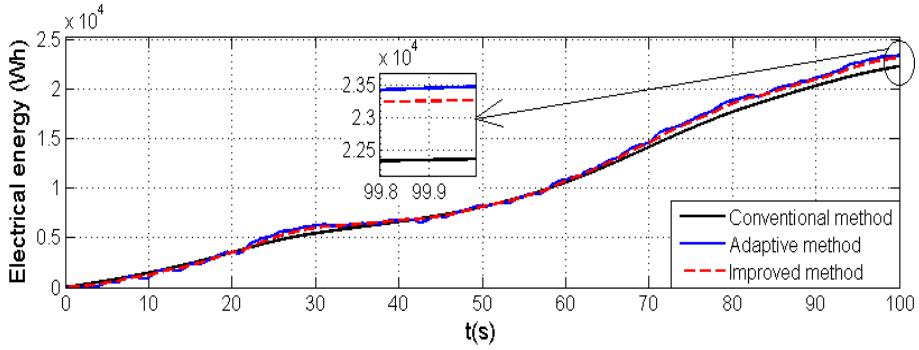

(d)

Fig. 4.5: Simulation results: (a) wind speed, (b) power coefficient, (c)error $P_{\max}(t) - P_m(t)$, and (d) energy output.

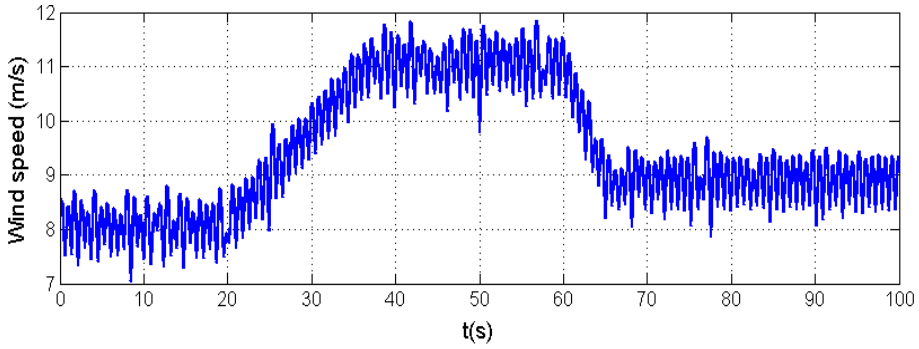

(a)

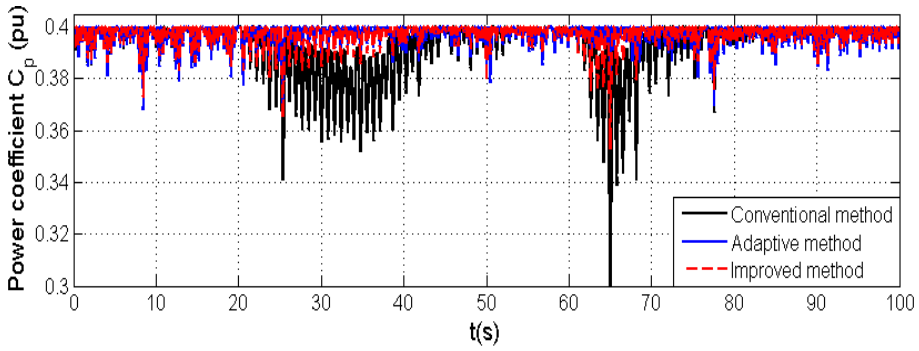

(b)

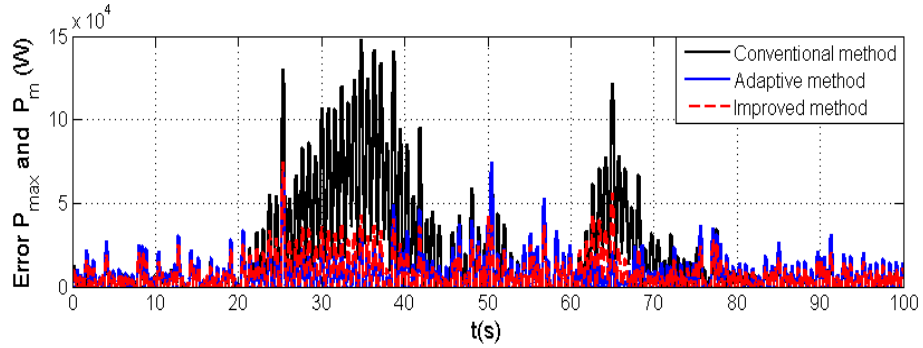

(c)

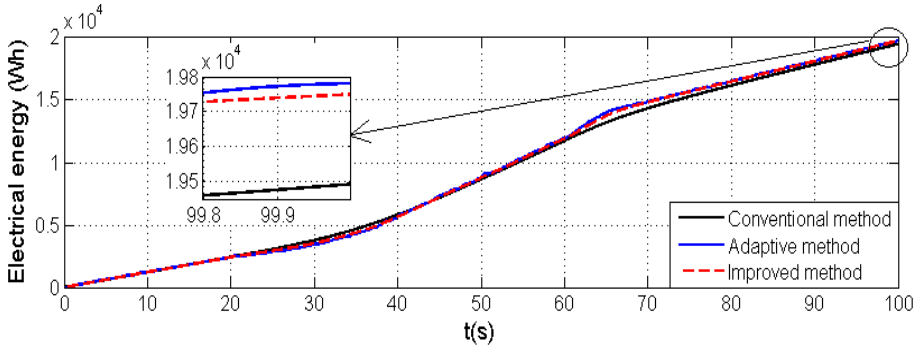

(d)

Fig. 4.6: Simulation results: (a) wind speed, (b) power coefficient, (c) error $P_{\max}(t) - P_m(t)$, and (d) energy output.

Chapter 5

Conclusion

In this dissertation, I proposed two methods including improved MPPT method and adaptive one, and respective control laws for the rotor side converter to obtain the maximum power point tracking of Doubly-fed induction generator (DFIG) wind turbine. Both methods do not require any information of wind data or wind sensor. Comparing to the first scheme, the second method does not require the precise parameters of the wind turbine. The MPPT capability of these proposed schemes is theoretically proven under some certain assumptions. The DFIG state-space model and control techniques based on the Lyapunov function are adopted to derive the RSC control methods corresponding to the proposed MPPT method. The quality of the proposed methods are verified by the numerical simulation of a 1.5-MW DFIG wind turbine. The simulation results show that the wind turbine implemented with these proposed methods can track the optimal operation point properly. Furthermore, the energy output of the DFIG wind turbine using the proposed methods is higher compared to the conventional MPPT-curve method under the same conditions.

Appendix A

DFIG Wind Turbine

A.1 Proof of Lemma 2

From Equations (2.24) and (2.14), (2.27) changes as follows:

$$\begin{aligned}\frac{d}{dt}\mathbf{x}_{pq}(t) &= -\tilde{V}_s\frac{d}{dt}\mathbf{i}_r(t) = -\mathbf{A}_i(t)\tilde{V}_s\mathbf{i}_r(t) - \frac{\tilde{V}_s}{\sigma}\mathbf{v}_r(t) - \tilde{V}_s\mathbf{d}_i(t)\\ &= \mathbf{A}_i(t)\mathbf{x}_{pq}(t) - \frac{\tilde{V}_s}{\sigma}\mathbf{v}_r(t) - \frac{\mathbf{A}_i(t)}{L_s\omega_s}\begin{bmatrix}V_s^2\\0\end{bmatrix} - \tilde{V}_s\mathbf{d}_i(t)\end{aligned}$$

By applying a transformation:

$$\mathbf{x}_{pq}(t) = \mathbf{C}(t)\mathbf{x}_{PQ}(t) \tag{A.1}$$

to Equation (2.27), we have:

$$\frac{d}{dt}\mathbf{x}_{pq}(t) = \dot{\mathbf{C}}(t)\mathbf{x}_{PQ}(t) + \mathbf{C}(t)\frac{d}{dt}\mathbf{x}_{PQ}(t) = \mathbf{A}_i(t)\mathbf{x}_{pq}(t) - \frac{\tilde{V}_s}{\sigma}\mathbf{v}_r(t) + \mathbf{c}_{pq}(t) \tag{A.2}$$

Hence, Equation (2.28) changes to be:

$$\frac{d}{dt}\mathbf{x}_{PQ}(t) = \mathbf{C}(t)^{-1}\left(\mathbf{A}_i(t)\mathbf{C}(t) - \dot{\mathbf{C}}(t)\right)\mathbf{x}_{PQ}(t) - \frac{\tilde{V}_s}{\sigma}\mathbf{C}(t)^{-1}\mathbf{v}_r(t) + \mathbf{C}(t)^{-1}\mathbf{c}_{pq}(t) \tag{A.3}$$

Here, it is easy to check Equations (2.32) and (2.30) by using:

$$\dot{\mathbf{C}}(t) = \begin{bmatrix}1 & 0\\ 0 & -\dfrac{\omega_s}{\omega_r(t)^2}\frac{d}{dt}\omega_r(t)\end{bmatrix} \tag{A.4}$$

Appendix B

Controller Design and Maximum Power Strategy

B.1 Proof of Lemma 3

From (3.14), for a point $(\omega_r, V_w) \in D_{\text{opt}}$, $\zeta(\omega_r, V_w) > 0$. For a point $(\omega_r, V_w) \in D_{\text{lr}}$, since $\lambda > \lambda_{\text{opt}}$, from (3.18), $C_p(\lambda) \leq C_{p\max}$,

$$\zeta(\omega_r, V_w) > \frac{\rho\pi R^6 \omega_r^2 C_p(\lambda)}{2V_w\lambda^3(\lambda - \lambda_{\text{opt}})}\left(\frac{\lambda^3}{\lambda_{\text{opt}}^3} - 1\right) > 0. \tag{B.1}$$

For a point $(\omega_r, V_w) \in D_{\text{ul}}$, since $\omega_r < \omega_{r\text{opt}}(V_w)$, it follows from (3.17) and (3.19) that $\zeta(\omega_r, V_w) > 0$.

B.2 Proof of Lemma 4

Let $\mathbf{e}_x(t) = \mathbf{x}_r(t) - \mathbf{x}_{PQ}(t)$. By applying (3.25) to (2.28), we have:

$$\frac{d}{dt}\mathbf{x}_{PQ}(t) = -\mathbf{P}\mathbf{e}_x(t) + \frac{d}{dt}\mathbf{x}_{\text{r}}(t) \tag{B.2}$$

which is equivalent to:

$$\frac{d}{dt}\mathbf{e}_x(t) = -\mathbf{P}\mathbf{e}_x(t) \tag{B.3}$$

It is obvious that when we define a Lyapunov function $V(e_x) = \mathbf{e}_x(t)^\top \mathbf{e}_x(t)$, its time derivative becomes:

$$\frac{d}{dt}V(\mathbf{e}_x) = 2\mathbf{e}_x(t)^\top \frac{d}{dt}\mathbf{e}_x(t) = -2\mathbf{e}_x(t)^\top \mathbf{P}\mathbf{e}_x(t) < 0 \tag{B.4}$$

for any $\mathbf{e}_x(t) \neq 0$. Hence, $\mathbf{e}_x(t)$ converges to zero.

B.3 Proof of Theorem 1

First, let $\mathbf{e}_x(t) = \begin{bmatrix} e_Q & e_P \end{bmatrix}^{\mathrm{T}} = \mathbf{x}_{\mathrm{r}}(t) - \mathbf{x}_{PQ}(t)$, $e_\lambda(t) = \lambda(t) - \lambda_{\mathrm{opt}}$. We define a Lyapunov candidate as

$$V(\mathbf{e}_x, e_\lambda) = \mathbf{e}_x(t)^\top \mathbf{e}_x(t) + e_\lambda^2(t). \tag{B.5}$$

The time derivative of the Lyapunov function is

$$\dot{V}(\mathbf{e}_x, e_\lambda) = 2\mathbf{e}_x(t)^\top \frac{d}{dt}\mathbf{e}_x(t) + 2e_\lambda \frac{d}{dt}e_\lambda. \tag{B.6}$$

Since $\lambda(t) = R\omega_r(t)/V_w(t)$, we have

$$\frac{d}{dt}\lambda(t) = \frac{\lambda(t)}{\omega_r(t)}\frac{d}{dt}\omega_r(t) - \frac{\lambda(t)}{V_w(t)}\frac{d}{dt}V_w(t). \tag{B.7}$$

From (2.2) and $e_P(t) = P_{e\mathrm{ref}}(t) - P_e(t)$, we have

$$\frac{d}{dt}\omega_r(t) = \frac{1}{J\omega_r(t)}(P_m(t) + e_P(t) - P_{e\mathrm{ref}}(t)). \tag{B.8}$$

By substituting $P_{e\mathrm{ref}}$ from Equations (3.27) into (B.8), we get

$$\frac{d}{dt}\omega_r(t) = \frac{1}{\eta\omega_r(t)}(P_m(t) - k_{\mathrm{opt}}\omega_r^3(t) + e_P(t)) \tag{B.9}$$

where $\eta = J - \alpha > 0$. By substituting Equations (3.21) into (B.9), we have

$$\frac{d}{dt}\omega_r(t) = \frac{1}{\eta\omega_r(t)}\left(e_P(t) - \zeta_p(t)e_\lambda(t)\right). \tag{B.10}$$

From (B.10) and (B.7), we have

$$e_\lambda(t)\frac{d}{dt}e_\lambda(t) = e_\lambda(t)\frac{d}{dt}\lambda(t) = \delta_1(t)(e_\lambda(t)e_P(t) - \zeta_p(t)e_\lambda^2(t)) - \frac{2\lambda(t)}{V_w(t)}e_\lambda(t)\frac{d}{dt}V_w(t) \tag{B.11}$$

where $\delta_1(t) = \dfrac{\lambda(t)}{\eta\omega_r^2(t)} > 0$. Since

$$2e_P(t)e_\lambda(t) \leq \chi^{-1}e_P^2(t) + \chi e_\lambda^2(t), \tag{B.12}$$

$$\left|\frac{d}{dt}V_w(t)\right| \leq \gamma\frac{R}{\lambda_{\mathrm{opt}}}, \tag{B.13}$$

$$-\frac{2\lambda(t)e_\lambda(t)}{V_w(t)}\frac{d}{dt}V_w(t) \leq \frac{2\lambda(t)e_\lambda(t)}{V_w(t)}\left|\frac{d}{dt}V_w(t)\right| \leq \frac{2\lambda(t)|e_\lambda(t)|}{V_w(t)}\frac{R}{\lambda_{\mathrm{opt}}}\gamma, \tag{B.14}$$

we have

$$2e_\lambda(t)\frac{d}{dt}\lambda(t) \leq \chi^{-1}\delta_1(t)e_P^2(t) - \delta_2(t)e_\lambda^2(t) + \delta_3(t)|e_\lambda(t)|, \tag{B.15}$$

where

$$\delta_2(t) := (2\zeta_p(t) - \chi)\delta_1(t) > 0,$$

and

$$\delta_3(t) := \frac{2\lambda(t)R\gamma}{\lambda_{\text{opt}}V_w(t)} \geq 0.$$

From (B.4) and (B.15), (B.6) becomes

$$\dot{V}(\mathbf{e}_x, e_\lambda) \leq -2\mathbf{e}_x(t)^\top \mathbf{P}\mathbf{e}_x(t) + \chi^{-1}\delta_1(t)e_P^2(t) - \delta_2(t)e_\lambda^2(t) + \delta_3(t)|e_\lambda(t)|. \tag{B.16}$$

Obviously,

$$-2\mathbf{e}_x(t)^\top \mathbf{P}\mathbf{e}_x(t) + \chi^{-1}\delta_1(t)e_P^2(t) = -\mathbf{e}_x(t)^\top \tilde{\mathbf{P}}\mathbf{e}_x(t) < 0.$$

Hence,

$$\dot{V}(\mathbf{e}_x, e_\lambda) \leq -\delta_2(t)|e_\lambda(t)|\left(|e_\lambda(t)| - \frac{\delta_3(t)}{\delta_2(t)}\right) \leq -\delta_2(t)|e_\lambda(t)|\left(|e_\lambda(t)| - \Delta_3\right), \tag{B.17}$$

where

$$\Delta_3 = \max\frac{\delta_3(t)}{\delta_2(t)} = 2\eta\gamma\frac{R}{\lambda_{\text{opt}}}\max\frac{\omega_r^2(t)}{(2\zeta_p(t) - \chi)V_w(t)}. \tag{B.18}$$

Then, $V(e_x, e_\lambda)$ decreases when:

$$|e_\lambda(t)| > \Delta_3 = 2\eta\gamma\frac{R}{\lambda_{\text{opt}}}\max\frac{\omega_r^2(t)}{(2\zeta_p(t) - \chi)V_w(t)}. \tag{B.19}$$

By multiplying two side of (B.19) by $\frac{V_{w\text{rated}}}{R}$, we have

$$|\omega_r(t) - \omega_{r\text{opt}}(t)| > \Delta_3\frac{V_{w\text{rated}}}{R} = 2\eta\gamma\frac{V_{w\text{rated}}}{\lambda_{\text{opt}}}\max\frac{\omega_r^2(t)}{(2\zeta_p(t) - \chi)V_w(t)}. \tag{B.20}$$

This completes the proof of Theorem 1.

B.4 Proof of Lemma 5

Remark 3. The inequality (3.33) means that $\tilde{\mathbf{Q}} = \tilde{\mathbf{Q}}^\top$ is a positive definite matrix. See B.5 for the definition and the related properties.

Proof. Let us define

$$\mathbf{e}_1(t) \triangleq \begin{bmatrix} e_{\omega_{r\mathrm{ref}}}(t) \\ \mathbf{e}_i(t) \end{bmatrix} = \begin{bmatrix} \omega_{r\mathrm{ref}}(t) - \omega_r(t) \\ \mathbf{i}_{r\mathrm{ref}}(t) - \mathbf{i}_r(t) \end{bmatrix}. \tag{B.21}$$

(3.32) can be rewritten as

$$k_d \frac{d}{dt} e_{\omega_{r\mathrm{ref}}}(t) = -k_p e_{\omega_{r\mathrm{ref}}}(t) + \begin{bmatrix} 0 & 1 \end{bmatrix} \mathbf{e}_i(t). \tag{B.22}$$

By substituting (3.31) into (2.14), we have

$$\frac{d}{dt} \left(\mathbf{i}_{r\mathrm{ref}}(t) - \mathbf{i}_r(t) \right) = -\mathbf{K} \left(\mathbf{i}_{r\mathrm{ref}}(t) - \mathbf{i}_r(t) \right). \tag{B.23}$$

Then,

$$\mathbf{E}_1 \frac{d}{dt} \mathbf{e}_1(t) = \mathbf{A}_1 \mathbf{e}_1(t), \tag{B.24}$$

where

$$\mathbf{E}_1 = \begin{bmatrix} k_d & \mathbf{0} \\ \mathbf{0} & \mathbf{I}_2 \end{bmatrix} > 0, \quad \mathbf{A}_1 = -\begin{bmatrix} k_p & \begin{bmatrix} 0 & -1 \end{bmatrix} \\ \mathbf{0} & \mathbf{K} \end{bmatrix}. \tag{B.25}$$

When we define a Lyapunov function as

$$V_1 \triangleq \mathbf{e}_1^\top(t) \mathbf{E}_1 \mathbf{e}_1(t), \tag{B.26}$$

its derivative is

$$\dot{V}_1 = \mathbf{e}_1^\top(t) \mathbf{E}_1 \frac{d}{dt} \mathbf{e}_1(t) + \left(\frac{d}{dt} \mathbf{e}_1(t) \right)^\top \mathbf{E}_1 \mathbf{e}_1(t). \tag{B.27}$$

By substituting (B.24) into (B.27), and noting that $\mathbf{A}_1 + \mathbf{A}_1^\top = -\tilde{\mathbf{Q}}$, we have

$$\dot{V}_1 = \mathbf{e}_1^\top(t) \left(\mathbf{A}_1 + \mathbf{A}_1^\top \right) \mathbf{e}_1(t) = -\mathbf{e}_1^\top(t) \tilde{\mathbf{Q}} \mathbf{e}_1(t) \leq -\lambda_{\min}(\tilde{\mathbf{Q}}) \mathbf{e}_1^\top(t) \mathbf{e}_1(t). \tag{B.28}$$

From the Lyapunov Stability Theory, $\lim_{t \to \infty} \mathbf{e}_1(t) = 0$. This completes the proof.

□

B.5 Matrix inequality

Let $\mathbf{S}^n$ denote a set of real-valued symmetrical $n \times n$ matrices and let $\lambda_i(\mathbf{Y})$ denote the ith eigenvalue of $\mathbf{Y} \in \mathbf{S}^n$.

For $\mathbf{Y} \in \mathbf{S}^n$ and $\mathbf{x} \in \mathbf{R}^n$, the following inequality holds [32]:

$$\min \lambda_i(\mathbf{Y}) \left\| \mathbf{x} \right\|^2 \leq \mathbf{x}^\top \mathbf{Y} \mathbf{x} \leq \max \lambda_i(\mathbf{Y}) \left\| \mathbf{x} \right\|^2. \tag{B.29}$$

Definition 1. (ex. p. 647 in [33]) A matrix $\mathbf{Y} = \mathbf{Y}^\top \in \mathbf{R}^{n\times n}$ is said to be *positive definite* if $\mathbf{x}^\top\mathbf{Y}\mathbf{x} > 0$ for all nonzero vector $\mathbf{x} \in \mathbf{R}^n$. We denote the positive definite matrix as $\mathbf{Y} > 0$. Moreover, if $\mathbf{x}^\top\mathbf{Y}\mathbf{x} \geq 0$ for all $\mathbf{x} \neq 0$, $\mathbf{Y}$ is said to be *positive semidefinite*, and we denote it as $\mathbf{Y} \geq 0$.

Lemma 7. For $\mathbf{Y} \in \mathbf{S}^n$,

$$\mathbf{Y} > 0 \quad \Leftrightarrow \quad \lambda_i(\mathbf{Y}) > 0, \tag{B.30}$$

$$\mathbf{Y} \geq 0 \quad \Leftrightarrow \quad \lambda_i(\mathbf{Y}) \geq 0. \tag{B.31}$$

For $\mathbf{Y},\ \mathbf{Z} \in \mathbf{S}^n$, we use $\mathbf{Y} > (\geq)\mathbf{Z}$ to mean $\mathbf{Y} - \mathbf{Z} > (\geq)0$.

Lemma 8. For any matrices $\mathbf{Y}$ and $\mathbf{Z}$,

$$\pm\mathbf{Y}^\top\mathbf{Z} \pm \mathbf{Z}^\top\mathbf{Y} \quad \leq \quad \mathbf{Y}^\top\mathbf{Y} + \mathbf{Z}^\top\mathbf{Z}, \tag{B.32}$$

$$\mp\mathbf{Y}^\top\mathbf{Z} \mp \mathbf{Z}^\top\mathbf{Y} \quad \geq \quad -\mathbf{Y}^\top\mathbf{Y} - \mathbf{Z}^\top\mathbf{Z}. \tag{B.33}$$

Proof. It is trivial from

$$\mp\mathbf{Y}^\top\mathbf{Z} \mp \mathbf{Z}^\top\mathbf{Y} + \mathbf{Y}^\top\mathbf{Y} + \mathbf{Z}^\top\mathbf{Z} = (\mathbf{Y} \mp \mathbf{Z})^\top(\mathbf{Y} \mp \mathbf{Z}) \geq 0. \tag{B.34}$$

□

Lemma 9.

$$\begin{bmatrix} \mathbf{Q} & \mathbf{S} \\ \mathbf{S}^\top & \mathbf{R} \end{bmatrix} > 0 \Leftrightarrow \quad \mathbf{R} > 0 \text{ and } \mathbf{Q} - \mathbf{S}\mathbf{R}^{-1}\mathbf{S}^\top > 0 \tag{B.35}$$

$$\Leftrightarrow \quad \mathbf{Q} > 0 \text{ and } \mathbf{R} - \mathbf{S}^\top\mathbf{Q}^{-1}\mathbf{S} > 0. \tag{B.36}$$

Proof.

$$\begin{bmatrix} \mathbf{Q} & \mathbf{S} \\ \mathbf{S}^\top & \mathbf{R} \end{bmatrix} = \begin{bmatrix} \mathbf{I} & \mathbf{S}\mathbf{R}^{-1} \\ \mathbf{0} & \mathbf{I} \end{bmatrix} \begin{bmatrix} \mathbf{Q} - \mathbf{S}\mathbf{R}^{-1}\mathbf{S}^\top & \mathbf{0} \\ \mathbf{0} & \mathbf{R} \end{bmatrix} \begin{bmatrix} \mathbf{I} & \mathbf{0} \\ \mathbf{R}^{-1}\mathbf{S}^\top & \mathbf{I} \end{bmatrix} \tag{B.37}$$

$$= \begin{bmatrix} \mathbf{I} & \mathbf{0} \\ \mathbf{S}^\top\mathbf{Q}^{-1} & \mathbf{I} \end{bmatrix} \begin{bmatrix} \mathbf{Q} & \mathbf{0} \\ \mathbf{0} & \mathbf{R} - \mathbf{S}^\top\mathbf{Q}^{-1}\mathbf{S} \end{bmatrix} \begin{bmatrix} \mathbf{I} & \mathbf{Q}^{-1}\mathbf{S} \\ \mathbf{0} & \mathbf{I} \end{bmatrix} \tag{B.38}$$

□

For square matrices $\mathbf{A}$ and $\mathbf{B}$, we denote a block-diagonal matrix as

$$\mathbf{A} \oplus \mathbf{B} \triangleq \begin{bmatrix} \mathbf{A} & \mathbf{0} \\ \mathbf{0} & \mathbf{B} \end{bmatrix}. \tag{B.39}$$

B.6 Proof of Lemma 6

The solutions of (3.38) and (3.39) are

$$\hat{\omega}_{r\text{opt}}(t) = e^{-k_3 t}\hat{\omega}_{r\text{opt}}(0) + k_3 \int_0^t e^{-k_3(t-\tau)}\omega_r(\tau)d\tau, \tag{B.40}$$

$$\hat{k}_{\text{opt}}(t) = e^{-k_4 t}\hat{k}_{\text{opt}}(0) + \int_0^t (-\omega_r(\tau)^2\hat{\omega}_{r\text{opt}}(\tau) + \omega_r(\tau)^3 + k_4 k'_{\text{opt}})e^{-(k_4-\tau)}d\tau. \tag{B.41}$$

Because $\omega_r(t) < \omega_{r\text{rated}}$, we have

$$\begin{aligned}
\left|\hat{\omega}_{r\text{opt}}(t)\right| &\le \left|e^{-k_3 t}\right|\left|\hat{\omega}_{r\text{opt}}(0)\right| + k_3\left|\int_0^t e^{-k_3(t-\tau)}\omega_r(\tau)d\tau\right| \\
&\le \left|e^{-k_3 t}\right|\left|\hat{\omega}_{r\text{opt}}(0)\right| + k_3\omega_{r\text{rated}}\left|\int_0^t e^{-k_3(t-\tau)}d\tau\right| \\
&\le \left|\hat{\omega}_{r\text{opt}}(0)\right| + (1 - e^{-k_3 t})\omega_{r\text{rated}} \\
&\le \left|\hat{\omega}_{r\text{opt}}(0)\right| + \omega_{r\text{rated}}
\end{aligned}$$

and

$$\begin{aligned}
&\left|\hat{k}_{\text{opt}}(t)\right| \\
&\le \left|e^{-k_4 t}\right|\left|\hat{k}_{\text{opt}}(0)\right| + \int_0^t \left|\omega_r(\tau)^2\right|\left|\hat{\omega}_{r\text{opt}}(\tau)\right| e^{-k_4(t-\tau)}d\tau + \int_0^t \left(\left|\omega_r(\tau)^3\right| + k_4 k'_{\text{opt}}\right) e^{-k_4(t-\tau)}d\tau \\
&\le \left|e^{-k_4 t}\right|\left|\hat{k}_{\text{opt}}(0)\right| + (\left|\hat{\omega}_{r\text{opt}}(0)\right| + \omega_{r\text{rated}}) \int_0^t \left|\omega_r(\tau)^2\right| e^{-k_4(t-\tau)}d\tau \\
&\quad + \int_0^t \left(\left|\omega_r(\tau)^3\right| + k_4 k'_{\text{opt}}\right) e^{-k_4(t-\tau)}d\tau \\
&\le \left|\hat{k}_{\text{opt}}(0)\right| + (1 - e^{-k_4 t})\left(k_4^{-1}\omega_{r\text{rated}}^3 + k'_{\text{opt}}\right) + \left(\left|\hat{\omega}_{r\text{opt}}(0)\right| + \omega_{r\text{rated}}\right)(1 - e^{-k_4 t})k_4^{-1}\omega_{r\text{rated}}^2 \\
&\le \left|\hat{k}_{\text{opt}}(0)\right| + k_4^{-1}\omega_{r\text{rated}}^3 + k'_{\text{opt}} + \left(\left|\hat{\omega}_{r\text{opt}}(0)\right| + \omega_{r\text{rated}}\right)k_4^{-1}\omega_{r\text{rated}}^2 \\
&\le \left|\hat{k}_{\text{opt}}(0)\right| + 2k_4^{-1}\omega_{r\text{rated}}^3 + k_4^{-1}\left|\hat{\omega}_{r\text{opt}}(0)\right|\omega_{r\text{rated}}^2 + k'_{\text{opt}}.
\end{aligned}$$

B.7 Proof of Theorem 2

To use

$$\mathbf{E} = \begin{bmatrix} k_d & \mathbf{0} \\ \mathbf{0} & \mathbf{I}_2 \end{bmatrix} \oplus \begin{bmatrix} \hat{J} & \mathbf{0} \\ \mathbf{0} & \mathbf{I}_2 \end{bmatrix} > 0 \tag{B.42}$$

and

$$\mathbf{X} = \begin{bmatrix} \alpha \mathbf{I}_3 & \mathbf{0} \\ \mathbf{0} & \mathbf{I}_3 \end{bmatrix} > 0, \tag{B.43}$$

we define a Lyapunov function as

$$V \triangleq \mathbf{e}(t)^\top \mathbf{X}\mathbf{E}\mathbf{e}(t), \tag{B.44}$$

where

$$\mathbf{e}(t) = \begin{bmatrix} e_{\omega_{r\text{ref}}}(t) \\ \mathbf{e}_i(t) \\ e_{\omega_{\text{opt}}}(t) \\ e_{\hat{\omega}_{r\text{opt}}}(t) \\ e_{k_{\text{opt}}}(t) \end{bmatrix} \triangleq \begin{bmatrix} \omega_{r\text{ref}}(t) - \omega_r(t) \\ \mathbf{i}_{r\text{ref}}(t) - \mathbf{i}_r(t) \\ \omega_r(t) - \omega_{r\text{opt}}(V_w(t)) \\ \omega_{r\text{opt}}(V_w(t)) - \hat{\omega}_{r\text{opt}}(t) \\ k_{\text{opt}} - \hat{k}_{\text{opt}}(t) \end{bmatrix}. \tag{B.45}$$

In this proof, we show that the derivative of the Lyapunov function

$$\dot{V} = \mathbf{e}(t)^\top \mathbf{X}\mathbf{E}\frac{d}{dt}\mathbf{e}(t) + \left(\mathbf{E}\frac{d}{dt}\mathbf{e}(t)\right)^\top \mathbf{X}\mathbf{e}(t), \tag{B.46}$$

satisfies

$$\dot{V} < -qV + \epsilon. \tag{B.47}$$

By defining the function $p(t) \triangleq -qV + \epsilon - \dot{V} > 0$, we have

$$\dot{V} = -qV + \epsilon - p(t).$$

Then,

$$V(t) = e^{-qt}V(0) + \int_0^t e^{-q(t-\tau)}\left(\epsilon - p(\tau)\right) d\tau \tag{B.48}$$

$$< e^{-qt}V(0) + \int_0^t e^{-q(t-\tau)}\epsilon d\tau \tag{B.49}$$

$$= e^{-qt}V(0) + \frac{\epsilon}{q}\left(1 - e^{-qt}\right). \tag{B.50}$$

Hence, the upper bound of $V(t)$ converges to ϵ/q. This implies that $V(t)$ will be bounded by ϵ/q as t increases. Since $\hat{J}e_{\omega_{\text{opt}}}(t)^2 \leq V(t)$, there exists a time $t_o > 0$ such that for all $t \geq t_o$,

$$|e_{\omega_{\text{opt}}}(t)| = |\omega_r(t) - \omega_{r\text{opt}}(V_w(t))| < \sqrt{\frac{\epsilon}{\hat{J}q}} \tag{B.51}$$

is satisfied.

Hereafter, we will derive (B.47).

From (2.2), (3.16), and (3.36), we have

$$\begin{aligned} J\omega_r(t)\frac{d}{dt}\omega_r(t) &= P_m(t) - P_e(t) \\ &= k_{\mathrm{opt}}\omega_r(t)^3 - \zeta(t)\omega_r(t)e_{\omega_{\mathrm{opt}}}(t) - \hat{k}_{\mathrm{opt}}(t)\omega_{r\mathrm{ref}}(t)^3 \\ &\quad + \omega_r(t)\left(k_1\frac{d}{dt}\omega_r(t) - k_2\left(\omega_r(t) - \hat{\omega}_{r\mathrm{opt}}(t)\right)\right). \end{aligned}$$

Then, when we use $\hat{J} = J - k_1$ and $\omega_{r\mathrm{ref}}(t)^3 - \omega_r(t)^3 = \xi\left(\omega_r(t), \omega_{r\mathrm{ref}}(t)\right)\omega_r(t)e_{\omega_{r\mathrm{ref}}}(t)$, and $\omega_r(t) - \hat{\omega}_{r\mathrm{opt}}(()t) = e_{\omega_{\mathrm{opt}}}(t) + e_{\hat{\omega}_{r\mathrm{opt}}}(t)$, we have

$$\begin{aligned} \hat{J}\frac{d}{dt}\omega_r(t) &= k_{\mathrm{opt}}\omega_r(t)^2 - \zeta(t)e_{\omega_{\mathrm{opt}}}(t) - \hat{k}_{\mathrm{opt}}(t)\omega_r(t)^2 \\ &\quad - \hat{k}_{\mathrm{opt}}(t)\xi\left(\omega_r(t), \omega_{r\mathrm{ref}}(t)\right)e_{\omega_{r\mathrm{ref}}}(t) - k_2\left(\omega_r(t) - \hat{\omega}_{r\mathrm{opt}}(t)\right) \\ &= (k_{\mathrm{opt}} - \hat{k}_{\mathrm{opt}}(t))\omega_r(t)^2 - \zeta(t)e_{\omega_{\mathrm{opt}}}(t) \\ &\quad - \hat{k}_{\mathrm{opt}}(t)\xi\left(\omega_r(t), \omega_{r\mathrm{ref}}(t)\right)e_{\omega_{r\mathrm{ref}}}(t) - k_2\left(e_{\omega_{\mathrm{opt}}}(t) + e_4(t)\right) \\ &= -\zeta(t)e_{\omega_{\mathrm{opt}}}(t) - k_2\left(e_{\omega_{\mathrm{opt}}}(t) + e_{\hat{\omega}_{r\mathrm{opt}}}(t)\right) \\ &\quad + \omega_r(t)^2 e_{k_{\mathrm{opt}}}(t) - \hat{k}_{\mathrm{opt}}(t)\xi\left(\omega_r(t), \omega_{r\mathrm{ref}}(t)\right)e_{\omega_{r\mathrm{ref}}}(t). \end{aligned}$$

Hence,

$$\begin{aligned} \hat{J}\frac{d}{dt}e_3(t) &= \hat{J}\frac{d}{dt}\omega_r(t) - \hat{J}\frac{d}{dt}\omega_{r\mathrm{opt}}(V_w(t)) \\ &= -\left(\zeta(t) + k_2\right)e_{\omega_{\mathrm{opt}}}(t) - k_2 e_{\hat{\omega}_{r\mathrm{opt}}}(t) + \omega_r(t)^2 e_{k_{\mathrm{opt}}}(t) \\ &\quad - \hat{k}_{\mathrm{opt}}(t)\xi\left(\omega_r(t), \omega_{r\mathrm{ref}}(t)\right)e_{\omega_{r\mathrm{ref}}}(t) - \hat{J}\frac{d}{dt}\omega_{r\mathrm{opt}}(V_w(t)). \end{aligned} \tag{B.52}$$

From (B.24), (3.35), (3.39), (3.38), and (B.52), we can summarize

$$\mathbf{E}\frac{d}{dt}\mathbf{e}(t) = \mathbf{A}(t)\mathbf{e}(t) + \mathbf{B}\frac{d}{dt}\omega_{r\mathrm{opt}}(t) + \mathbf{C}\delta + \mathbf{D}\hat{k}_{\mathrm{opt}}(t)\xi\left(\omega_r(t), \omega_{r\mathrm{ref}}(t)\right)\mathbf{G}\mathbf{e}(t), \tag{B.53}$$

where

$$\mathbf{A}(t) = \begin{bmatrix} \mathbf{A}_1 & \mathbf{0} \\ \mathbf{0} & \mathbf{A}_2(t) \end{bmatrix},\ \mathbf{B} = \begin{bmatrix} 0 \\ 0 \\ -\hat{J} \\ 1 \\ 0 \end{bmatrix}, \mathbf{C} = \begin{bmatrix} 0 \\ 0 \\ 0 \\ 0 \\ -k_4 \end{bmatrix}, \mathbf{D} = \begin{bmatrix} 0 \\ 0 \\ -1 \\ 0 \\ 0 \end{bmatrix},\ \mathbf{G} = \begin{bmatrix} 1 & 0 & 0 & 0 & 0 \end{bmatrix},$$

$$\mathbf{A}_1 = -\begin{bmatrix} k_p & \begin{bmatrix} 0 & -1 \end{bmatrix} \\ \mathbf{0} & \mathbf{K} \end{bmatrix}, \mathbf{A}_2(t) = \begin{bmatrix} -(\zeta(t) + k_2) & -k_2 & J\omega_r(t)^2 \\ -k_3 & -k_3 & 0 \\ -\omega_r(t)^2 & -\omega_r(t)^2 & -k_4 \end{bmatrix}. \tag{B.54}$$

By substituting (B.53) into (B.46), we have

$$\begin{aligned} \dot{V} = {} & \mathbf{e}(t)^\top \left(\mathbf{X}\mathbf{A}(t) + \mathbf{A}(t)^\top \mathbf{X}\right) \mathbf{e}(t) + 2\mathbf{e}(t)^\top \mathbf{X}\mathbf{B} \frac{d}{dt}\omega_{r\mathrm{opt}}(t) \\ & + 2\mathbf{e}(t)^\top \mathbf{C}\delta + 2\mathbf{e}(t)^\top \mathbf{X}\mathbf{D}\hat{k}_{\mathrm{opt}}(t)\xi\left(\omega_r(t), \omega_{r\mathrm{ref}}(t)\right)\mathbf{G}\mathbf{e}(t). \end{aligned} \tag{B.55}$$

Since $2|e_{\omega_{\mathrm{opt}}}(t)| \le we_{\omega_{\mathrm{opt}}}(t)^2 + w^{-1}$ and $2|e_{\hat{\omega}_{r\mathrm{opt}}}(t)| \le we_{\hat{\omega}_{r\mathrm{opt}}}(t)^2 + w^{-1}$ for $w > 0$, we have

$$\begin{aligned} 2\mathbf{e}(t)^\top \mathbf{X}\mathbf{B}\frac{d}{dt}\omega_{r\mathrm{opt}}(t) &\le 2\left|-\hat{J}e_{\omega_{\mathrm{opt}}}(t) + e_{\hat{\omega}_{r\mathrm{opt}}}(t)\right| \left|\frac{d}{dt}\omega_{r\mathrm{opt}}(V_w(t))\right| \\ &\le 2\left(\hat{J}|e_{\omega_{\mathrm{opt}}}(t)| + |e_{\hat{\omega}_{r\mathrm{opt}}}(t)|\right)\gamma \\ &\le \left(w\hat{J}e_{\omega_{\mathrm{opt}}}(t)^2 + we_{\hat{\omega}_{r\mathrm{opt}}}(t)^2 + w^{-1}\hat{J} + w^{-1}\right)\gamma \\ &= \mathbf{e}(t)^\top \mathbf{M}\mathbf{e}(t) + \epsilon_1, \end{aligned} \tag{B.56}$$

where

$$\mathbf{M} \triangleq w\gamma \mathrm{diag}\left(0, 0, \hat{J}, 1, 0\right), \tag{B.57}$$

$$\epsilon_1 \triangleq w^{-1}\gamma(\hat{J} + 1). \tag{B.58}$$

Likely, we have

$$2\mathbf{e}(t)^\top \mathbf{X}\mathbf{C}\delta < 2k_4|e_{k_{\mathrm{opt}}}(t)||\delta_{\max}|k_{\mathrm{opt}} \le \mathbf{e}(t)^\top \mathbf{N}\mathbf{e}(t) + \epsilon_2, \tag{B.59}$$

where $\mathbf{N} = \mathrm{diag}(0, 0, 0, 0, vk_{\mathrm{opt}}k_4)$, $\epsilon_2 = v^{-1}k_4k_{\mathrm{opt}}\delta_{\max}^2$. Furthermore, by applying

(B.32) in Lemma 8 to set $\mathbf{Y} = \alpha\hat{k}_{\text{opt}}(t)\xi\left(\omega_r(t), \omega_{r\text{ref}}(t)\right)\mathbf{G}$ and $\mathbf{Z} = \alpha^{-1}\mathbf{D}^\top\mathbf{X}$, we have

$$
\begin{aligned}
&2\mathbf{e}(t)^\top\mathbf{X}\mathbf{D}\hat{k}_{\text{opt}}(t)\xi\left(\omega_r(t), \omega_{r\text{ref}}(t)\right)\mathbf{G}\mathbf{e}(t) \\
&= \mathbf{e}(t)^\top\mathbf{G}^\top\hat{k}_{\text{opt}}(t)\xi\left(\omega_r(t), \omega_{r\text{ref}}(t)\right)\mathbf{D}^\top\mathbf{X}\mathbf{e}(t) + \mathbf{e}(t)^\top\mathbf{X}\mathbf{D}\hat{k}_{\text{opt}}(t)\xi\left(\omega_r(t), \omega_{r\text{ref}}(t)\right)\mathbf{G}\mathbf{e}(t) \\
&\leq \mathbf{e}(t)^\top\alpha^2\hat{k}_{\text{opt}}(t)^2\xi\left(\omega_r(t), \omega_{r\text{ref}}(t)\right)^2\mathbf{G}^\top\mathbf{G}\mathbf{e}(t) + \alpha^{-2}\mathbf{e}(t)^\top(t)\mathbf{X}\mathbf{D}\mathbf{D}^\top\mathbf{X}\mathbf{e}(t). \qquad \text{(B.60)}
\end{aligned}
$$

Then, by noting that $\alpha^{-2}\mathbf{X}\mathbf{D}\mathbf{D}^\top\mathbf{X} = \mathbf{D}\mathbf{D}^\top$ and defining

$$
\mathbf{Q}(t) \triangleq -\mathbf{X}\mathbf{A}(t) - \mathbf{A}(t)^\top\mathbf{X} - \mathbf{M} - \mathbf{N} - \mathbf{D}\mathbf{D}^\top - \alpha^2\hat{k}_{\text{opt}}(t)^2\xi\left(\omega_r(t), \omega_{r\text{ref}}(t)\right)^2\mathbf{G}^\top\mathbf{G}, \qquad \text{(B.61)}
$$

$$
\epsilon \triangleq \epsilon_1 + \epsilon_2, \qquad \text{(B.62)}
$$

we have

$$
\dot{V} \leq -\mathbf{e}(t)^\top\mathbf{Q}(t)\mathbf{e}(t) + \epsilon. \qquad \text{(B.63)}
$$

Hence, if

$$
\mathbf{Q}(t) - q\mathbf{X}\mathbf{E} > 0, \qquad \text{(B.64)}
$$

then

$$
\dot{V} < -q\mathbf{e}(t)^\top\mathbf{X}\mathbf{E}\mathbf{e}(t) + \epsilon. \qquad \text{(B.65)}
$$

This implies (B.47). To complete the proof, we need the next lemma.

Lemma 10. The five inequalities in (3.44) imply (B.64).

Proof. $q\mathbf{X}\mathbf{E}$ and $\mathbf{Q}(t)$ are both block diagonal as

$$
q\mathbf{X}\mathbf{E} = q\alpha\begin{bmatrix} k_d & \mathbf{0} \\ \mathbf{0} & \mathbf{I}_2 \end{bmatrix} \oplus q\begin{bmatrix} \hat{J} & \mathbf{0} \\ \mathbf{0} & \mathbf{I}_2 \end{bmatrix}, \qquad \text{(B.66)}
$$

$$
\begin{aligned}
\mathbf{Q}(t) = \alpha&\begin{bmatrix} 2k_p - \alpha\hat{k}_{\text{opt}}(t)^2\xi\left(\omega_r(t), \omega_{r\text{ref}}(t)\right)^2 & \begin{bmatrix} 0 & -1 \end{bmatrix} \\ \begin{bmatrix} 0 \\ -1 \end{bmatrix} & \mathbf{K}^\top + \mathbf{K} \end{bmatrix} \\
&\oplus \begin{bmatrix} 2\zeta(t) + 2k_2 - w\gamma\hat{J} - 1 & k_2 + k_3 & 0 \\ k_2 + k_3 & 2k_3 - w\gamma & \omega_r(t)^2 \\ 0 & \omega_r(t)^2 & (2 - vk_{\text{opt}})k_4 \end{bmatrix}. \qquad \text{(B.67)}
\end{aligned}
$$

Hence, we show (B.64) separately as

$$\begin{bmatrix} 2k_p - \alpha\hat{k}_{\text{opt}}(t)^2\xi\left(\omega_r(t), \omega_{r\text{ref}}(t)\right)^2 & \begin{bmatrix} 0 & -1 \end{bmatrix} \\ \begin{bmatrix} 0 \\ -1 \end{bmatrix} & \mathbf{K}^\top + \mathbf{K} \end{bmatrix} - q \begin{bmatrix} k_d & \mathbf{0} \\ \mathbf{0} & \mathbf{I}_2 \end{bmatrix} > 0, \tag{B.68}$$

$$\begin{bmatrix} 2\zeta(t) + 2k_2 - w\gamma\hat{J} - 1 & k_2 + k_3 & 0 \\ k_2 + k_3 & 2k_3 - w\gamma & \omega_r(t)^2 \\ 0 & \omega_r(t)^2 & (2 - vk_{\text{opt}})k_4 \end{bmatrix} - q \begin{bmatrix} \hat{J} & \mathbf{0} \\ \mathbf{0} & \mathbf{I}_2 \end{bmatrix} > 0. \tag{B.69}$$

By noting that $\hat{k}_{\text{opt,ub}}\xi_{\max} \geq \hat{k}_{\text{opt}}(t)\xi\left(\omega_r(t), \omega_{r\text{ref}}(t)\right)$ and applying (9) , the first two inequalities in (3.44) imply (B.68).

$$\begin{cases} 2k_p - \alpha\hat{k}^2_{\text{opt,ub}}\xi^2_{\max} - \begin{bmatrix} 0 & -1 \end{bmatrix} \mathbf{\Xi}^{-1} \begin{bmatrix} 0 \\ -1 \end{bmatrix} - qk_d > 0, \\ \mathbf{\Xi} = \mathbf{K}^\top + \mathbf{K} - q\mathbf{I}_2 > 0. \end{cases} \tag{B.70}$$

To apply (B.33) in Lemma 8 by setting

$$\mathbf{Y} = \begin{bmatrix} \sqrt{k_2 + k_3} & 0 & 0 \\ 0 & 0 & \omega_r(t) \end{bmatrix}, \ \mathbf{Z} = \begin{bmatrix} 0 & \sqrt{k_2 + k_3} & 0 \\ 0 & \omega_r(t) & 0 \end{bmatrix}, \tag{B.71}$$

the off-diagonal elements of (B.69) are bounded as

$$\begin{bmatrix} 0 & k_2 + k_3 & 0 \\ k_2 + k_3 & 0 & \omega_r(t)^2 \\ 0 & \omega_r(t)^2 & 0 \end{bmatrix} \geq - \begin{bmatrix} k_2 + k_3 & 0 & 0 \\ 0 & k_2 + k_3 + \omega_r(t)^2 & 0 \\ 0 & 0 & \omega_r(t)^2 \end{bmatrix}. \tag{B.72}$$

By noting that $\zeta(t) \geq \zeta_{\min}$ and $\omega_r(t) \leq \omega_{r\text{rated}}$, the last three inequalities in (3.44) imply (B.69).

$$\begin{cases} 2\zeta_{\min} - w\hat{J}\gamma - (k_3 - k_2) - 1 > q\hat{J}, \\ k_3 - k_2 - \omega^2_{r\text{rated}} - w\gamma > q, \\ (2 - vk_{\text{opt}})k_4 - \omega^2_{r\text{rated}} > q. \end{cases} \tag{B.73}$$

Remark 4. We consider $\xi\left(\omega_r, \omega_{r\text{ref}}\right)$ only for the region of $\omega_r > 0$ and $\omega_{r\text{ref}} > 0$, and the Hessian of $\xi\left(\omega_r, \omega_{r\text{ref}}\right)$ is positive semidefinite as

$$\begin{bmatrix} \dfrac{\partial^2\xi}{\partial\omega_r^2} & \dfrac{\partial^2\xi}{\partial\omega_r\partial\omega_{r\text{ref}}} \\ \dfrac{\partial^2\xi}{\partial\omega_{r\text{ref}}\partial\omega_r} & \dfrac{\partial^2\xi}{\partial\omega^2_{r\text{ref}}} \end{bmatrix} = 2 \begin{bmatrix} \dfrac{\omega^2_{r\text{ref}}}{\omega_r^3} & -\dfrac{\omega_{r\text{ref}}}{\omega_r^2} \\ -\dfrac{\omega_{r\text{ref}}}{\omega_r^2} & \dfrac{1}{\omega_r} \end{bmatrix} \geq 0. \tag{B.74}$$

Hence, $\xi_{\max}$ is attained at the boundary of the region $[\omega_{r\min}, \omega_{r\text{rated}}] \times [\omega_{r\min}, \omega_{r\text{rated}}]$. Moreover, from

$$\begin{bmatrix} \dfrac{\partial \xi}{\partial \omega_r} \\ \dfrac{\partial \xi}{\partial \omega_{r\text{ref}}} \end{bmatrix} = \begin{bmatrix} 1 - \dfrac{\omega_{r\text{ref}}^2}{\omega_r^2} \\ 1 + 2\dfrac{\omega_{r\text{ref}}}{\omega_r} \end{bmatrix}, \tag{B.75}$$

it is easy to realize $\xi_{\max} = \xi(\omega_{r\min}, \omega_{r\text{rated}})$.

This completes the proof. □

Publications

Journal papers

[1] Dinh-Chung Phan, Shigeru Yamamoto: Maximum Energy Output of a DFIG Wind Turbine Using an Improved MPPT-Curve Method. *Energies*, 2015; 8: 11718-11736.

[2] Dinh-Chung Phan, Shigeru Yamamoto: Rotor Speed Control of Doubly Fed Induction Generator Wind Turbines Using Adaptive Maximum Power Point Tracking, *Energy*, 111 (2016), 377-388.

Bibliography

[1] http://www.gwec.net/wp-content/uploads/2016/04/GWEC_Global_Wind_2015_Report_LR-2.pdf(accessed on 9 April 2016)

[2] Xie D., Xu Z., Yang L., Ostergaard J., Xue Y, Wong K.P., A comprehensive LVRT control strategy for DFIG wind turbines with enhanced reactive power support. IEEE Trans. Power Syst. 2013; 28(3): 3302-3310.

[3] Alizadeh M., Kojori S.S., Augmenting effectiveness of control loops of a PMSG (permanent magnet synchronous generator) based wind energy conversion system by a virtually adaptive PI (proportional integral) controller. Energy 2015; 91: 610-629.

[4] Ganjefar S., Ghasemi A.A., A novel-strategy controller design for maximum power extraction in stand-alone windmill systems. Energy 2014; 76: 326-335.

[5] Barakati S.M., Kazerani M., Aplevich J.D., Maximum power tracking control for a wind turbine system including a matrix converter. IEEE Trans. Energy Convers. 2009; 24(3): 705-713.

[6] Lei Y., Mullane A., Lightbody G., Yacamini R., Modeling of the wind turbine with a doubly fed induction generator for grid integration studies. IEEE Trans. Energy Convers. 2006; 21(1): 257-264.

[7] Abdullah M., Yatim A.H.M., Tan C., Saidur R., A review of maximum power point tracking algorithms for wind energy systems. Renew. Sustain. Energy Rev. 2012; 16(5): 3220-3227.

[8] Ganjefar S., Ghassemi A., Ahmadi M., Improving efficiency of two-type maximum power point tracking methods of tip-speed ratio and optimum torque in wind turbine system using a quantum neural network. Energy 2014; 67: 444-453.

[9] Jeong H.G., Seung R.H., Lee K.B., An improved maximum power point tracking method for wind power systems. Energies 2012; 5: 1339-1354.

[10] Phan D.C., Ro K.S., Point of common coupling voltage recovery capability improvement of offshore wind farm connected to a weak grid through high voltage direct current link. J. Renew. Sustain. Energy 2012; 4: 063109(1-13).

[11] Tapia A., Tapia G., Ostolaza J., Saenz J., Modeling and control of a wind turbine driven doubly fed induction generator. IEEE Trans. Energy Convers. 2003; 18(2): 194-204.

[12] Fernandez L., Garcia C., Jurado F., Comparative study on the performance of control systems for doubly fed induction generator (DFIG) wind turbines operating with power regulation. Energy 2008; 33(9): 1438-1452.

[13] Yang L., Xu Z., stergaard J., Dong Z.Y., Wong K.P., Advanced control strategy of DFIG wind turbines for power system fault ride through. IEEE Trans. Power Syst. 2012; 27(2): 713-722.

[14] Wagner H., Mathur J., Introduction to wind energy systems: Basics, technology and operation. 2nd ed. Operation and control of wind energy converters, New York: Springer-Verlag; 2013, p. 63-64.

[15] Belmokhtar K., Doumbia M.L., Agbossou K., Novel fuzzy logic based sensorless maximum power point tracking strategy for wind turbine systems driven DFIG (doubly-fed induction generator). Energy 2014; 76: 679-693.

[16] Yang L., Xu Z., stergaard J., Dong Z.Y., Wong K.P, Ma X., Oscillatory stability and eigenvalue sensitivity analysis of a DFIG wind turbine system. IEEE Trans. Energy Convers. 2011; 26(1): 328-339.

[17] Mishra Y., Mishra S., Li F., Dong Z.Y., Bansal R.C., Small signal stability analysis of a DFIG-based wind power system under different modes of operation. IEEE Trans. Energy Convers. 2009; 24(4): 972-982.

[18] Hu J., Nian H., Hu B., He Y., Zhu Z.Q., Direct active and reactive power regulation of DFIG using sliding-mode control approach. IEEE Trans. Energy Convers.2010; 25(4): 1028-1039.

[19] Khemiri N., Khedher A., Mimouni M.F., Wind energy conversion system using DFIG controlled by backstepping and sliding mode strategies. Int. J. Renew. Energy Res. 2012; 2(3): 421-430.

[20] Lin W., Hong C., Cheng F., On-line designed hybrid controller with adaptive observer for variable-speed wind generation system. Energy 2010; 35: 3022-3030.

[21] Evangelista C., Puleston P., Valenciaga F., Fridman L.M., Lyapunov-designed super-twisting sliding mode control for wind energy conversion optimization. IEEE Trans. Ind. Electron. 2013; 60(2): 438-454.

[22] Barambones O., Durana J.M.G., Sen M.D., Robust speed control for variable speed wind turbine. Int. J. Innov. Comput. Inform. Contr. 2012; 8(11): 7627-7640.

[23] Beltran B., Ahmed-Ali T., Benbouzid M., High-order sliding-mode control of variable-speed wind turbines. IEEE Trans. Ind. Electron. 2009; 56(9): 3314-3321.

[24] `http://www.aweo.org/windmodels.html` (Accessed 9th December 2016)

[25] Wu B., Lang Y., Zargari N., Kouro S., Power conversion and control of wind energy system. Hoboken, New Jersey: John Wiley & Sons; 2011.

[26] Abad G., López J., Rodríguez M.A., Marroyo L., Iwanski G., Doubly fed induction machine: Modelling and control for wind energy generation. Hoboken, New Jersey: John Wiley & Sons; 2011.

[27] Hughes F. M., Anaya-Lara O., Jenkins N., Strbac G., A power system stabilizer for DFIG-based wind generation. IEEE Trans. Power Syst. 2006; 21: 763-772.

[28] González L.G., Figueres E., Garcerá G., Carranza O., Maximum-power-point tracking with reduced mechanical stress applied to wind-energy-conversion-systems. Appl. Energy 2010; 87: 2304-2312.

[29] Ghaffari A., Krstic M., Seshagiri S., Power optimization and control in wind energy conversion systems using extremum seeking. IEEE Trans. Control Syst. Tech. 2014; 22(5): 1684-1695.

[30] Qiao W., Yang X., Gong X., Wind speed and rotor position sensorless control for direct-drive PMG wind turbines. IEEE Trans. Ind. Appl. 2012; 48(1): 3-11.

[31] Qiao W., Zhou W., Aller J.M., Harley R.G., Wind speed estimation based sensorless output maximization control for a wind turbine driving a DFIG. IEEE Trans. Power. Electron. 2008; 23(3): 1156-1169.

[32] Boyd S., Ghaoui L. E.l., Feron E., Balakrishnan V., Linear matrix inequalities in system and control theory. Philadelphia: SIAM; 1994.

[33] Boyd S., Vandenberghe L., Convex optimization. New York: Cambridge University Press; 2004.